PRE-PRINT of the paper published on Desalination 452 (2019). Note that it may differ from the final published version (https://doi.org/10.1016/j.desal.2018.10.026) due to several revisions implemented during the peer review process of the journal.

New considerations for modelling a MED-TVC plant under dynamic conditions

L. Guimard[a,b], A. Cipollina[c*], B. Ortega-Delgado[c], G. Micale[c], F. Couenne[b], P. Bandelier[a], C. Jallut[b]

[a]Univ Grenoble Alpes, CEA, LITEN, Département Thermique Biomasse et Hydrogène, Laboratoire des Systèmes Solaires et Thermodynamiques, F-38000 Grenoble
[b]Univ Lyon, Université Claude Bernard Lyon 1, CNRS, LAGEP UMR 5007, 43 boulevard du 11 novembre 1918, F-69100, VILLEURBANNE, France
[c]Dipartimento dell'Innovazione Industriale e Digitale (DIID), Università di Palermo (UNIPA) – viale delle Scienze Ed.6, 90128 Palermo, Italy.
**e-mail: andrea.cipollina@unipa.it*

Abstract

The multiple-effect distillation (MED) technology is nowadays the most promising desalination process to be coupled with variable heat sources, thus leading to a more sustainable way to produce water. In order to prove the potential of this, it is of major interest to develop powerful modelling tools to predict the performance of this coupling. Only a few models have been presented so far. They show promising results but were based on some simplifying assumptions and non-physical constraints that could limit the analysis of the dynamic behaviour of a MED plant. This paper presents new considerations for the dynamic modelling of a MED plant associated with a thermal vapour compression unit , starting from a previous work "A dynamic model for MED-TVC transient operation". After several improvements, this model is now more representative of the real operating modes of a MED-TVC plant by considering real process inputs. This paper also highlights the importance of accurately modelling the interconnection between effects, the evaporation and condensation processes and the other components, such as the pre-heaters. Here is also presented a control strategy for operating a MED plant under dynamic conditions. Indeed, when a perturbation occurs in the motive steam pressure, it is possible to stabilise the whole plant by a simultaneous variation in the intake seawater mass flow rate at the final condenser. The model has been validated in steady-state conditions with experimental data from a MED-TVC plant operated in Trapani (Sicily) and was used to perform dynamic simulation to prove the feasibility of operating a MED-TVC plant under dynamic conditions, which is a major step toward proving the possibility of a coupling with renewable energies.

Keywords: dynamic model, transient operation, desalination, control strategy

1. Introduction

The longevity of human kind is directly linked to water resources. Demand for water will continue to increase over the next decades, mainly because of the growth of population, changes in lifestyles and consumption patterns. This will lead to more stress on limited natural resources and ecosystems. Hence, it is highly important to find a sustainable way to increase the production of water for domestic needs as well as for energy, agricultural and industrial purposes [1,2]
Several techniques are used to produce fresh water from seawater such as reverse osmosis (RO) or thermal processes like multiple-effect distillation (MED) and Multi Stage Flash (MSF). Due to its high energetic performances and flexibility, the former is considered as the best thermal process to be coupled with renewable energy sources [3].

PRE-PRINT of the paper published on Desalination 452 (2019). Note that it may differ from the final published version (https://doi.org/10.1016/j.desal.2018.10.026) due to several revisions implemented during the peer review process of the journal.

A multiple-effect distillation plant is made of a cascade of stages or effects, where a sequence of simultaneous evaporation and condensation processes takes place. Steam is introduced in the first effect where it is condensed inside a tube bundle. Thus, transferring the latent heat of condensation to the feed seawater sprayed over the external surface of the tubes, which reaches saturation conditions and evaporates. The produced vapour is used as the heating source for the next effect where the pressure is reduced stage by stage, then the above described process is repeated until the last effect. The accumulated brine in each effect flows toward the following one and flashes, therefore producing an additional amount of steam. Finally, the steam produced in the last effect is condensed in the final condenser, where the feed seawater is also pre-heated, thus, recovering part of the condensation heat and enhancing the overall process thermal efficiency.

MED plants are often coupled with a Thermal Vapour Compression (MED-TVC) as this can lead to an increase of 30-40% of the energetic performance of the plant [4]. High- or medium- pressure steam is injected into the steam ejector and is mixed with a part of the steam produced in one of the effects (in this work, the vapour is taken from the last effect). The exiting vapour is then used as the heating steam in the first effect.

The thermal energy required for the operation of the plant is mostly due to the production of the heating steam for the first effect. In most cases, it comes from fossil fuels, thus the coupling of a MED plant with renewable energy sources would create a more sustainable way of producing water. In this case, the main concern regards the behaviour of the MED plant under dynamic conditions due to the intermittent character of renewable energy sources. Therefore, it is fundamental to develop a model that is as accurate and close to reality as possible to prove its operability and potential when the available thermal power varies. For the sake of brevity, the following literature review only focuses on the works of specific interest for the present paper, while an exhaustive literature analysis for transient and steady-state MED modelling has been provided in [4].

Many steady-state models have been published, covering a wide variety of plant configurations, a lot of them are based on the work of El-Dessouky *et al.*[5–8], who also developed several useful correlations for the thermodynamic properties of seawater. Another valuable contribution was their work on the different ways of modelling the steam ejector for desalination applications [5,9]. Indeed, El-Dessouky *et al*. developed different models, depending on the information available for describing the steam ejector.

Even if valuable information can be obtained with steady-state simulations, it becomes more and more important to study the MED plant behaviour under transient conditions. With this respect, few studies on dynamic MED modelling have been published. One of the first model was presented by El-Nashar *et al.* [10] in 1990, who used a simplified dynamic model, r representing the temperatures' dynamics to analyze the transient behaviour of a multiple-effect stack-type distillation. Their results were compared to experimental data obtained from a plant operated in Abu Dhabi (UAE) with reasonable agreement.

In 1997, Aly and Marwan [11] proposed a new model for dynamic studies of MED processes and performed an interesting sensitivity analysis of the plant operation (temperature and brine salinity) to input disturbances, such as temperature and feed seawater mass flow rate variations. They decomposed each effect in three different control volumes: the vapour space, brine pool and tube bundle. For each one, they developed mass, energy and salt conservation differential equations. However, they made some simplifying assumptions, such as the absence of non-condensable gases (NCG) and did not consider the possibility of partial condensation inside the tubes bundles in each effect.

In 2005, Dardour *et al.* [12] developed a computer-package for MED plant modelling. Dardour *et al.* used this tool to study the coupling of a MED plant with a nuclear reactor. As well as most of the published works, their model is based on mass and energy balances and correlations are used for estimating the heat transfer coefficients and physical properties of seawater and pure water. Several simplifying assumptions, as mentioned for the previous work, were made.

Roca *et al.* [13] developed in 2008 a dynamic model for automatic operations of a solar-assisted MED pilot unit operating at Plataforma Solar de Almeria (PSA). The model was implemented in the object-oriented Modelica language. Their model was used to optimize the distillate production of the plant, despite several assumptions such as neglecting the impact of non-condensable gases, constant physical properties, constant difference of temperature between two successive effects and no possibility of brine accumulation in the effects.

In 2014, Mazini *et al.* [14] published an improved version of the model developed by Aly and Marwan [11]. They also modelled the steam ejector using empirical correlations presented by El-Dessouky *et al.* [9]. In this work, the steam flow is expressed with the energy balances, thus leading to a complete condensation in the tubes bundle and a lack of accumulation terms. Simulations results were used to perform analysis to determine the time variation of brine levels and other outputs. The model was validated with steady-state data from a real plant, with an error above 20% regarding the distillate production.

In 2014 and 2015, De la Calle *et al.* [15,16] presented a dynamic model for the pilot MED plant at PSA that uses a compound solar collector solar field as the thermal source. This model is based on the one developed by Roca *et al.* [13], and was implemented using the equation-based object-oriented Modelica language. In this work, they dissociated the condensation and the evaporation processes and took into account the accumulation of energy inside the tube bundle walls. However, Roca *et al.* did not consider some major phenomena that can greatly affect the plant behaviour under transient conditions, such as the presence of NCG or the accumulation of brine and vapour in each effect. Notwithstanding such assumptions, and by properly calibrating some parameters, their model has been validated with a good agreement. In 2016, Roca *et al*. [17] also published a linear model of a MED plant that was validated against a dynamic model [16] with a very good agreement and low computational effort. In this paper, the MED plant is connected to a greenhouse with daily variation of irrigation water demand.

More recently, Azimibavil and Dehkordi [18] published a dynamic model of MED processes with a special focus on the way the water and steam behave in one effect. They also consider the possibility of partial condensation in the tubes bundles and the thickness variation of the seawater film around the tubes for the falling film evaporator. Those results were used to characterize the fluids flows distributions.

The most recent work was presented by Cipollina *et al.* [4]. They aimed to address several gaps in the literature. Therefore, they implemented equations for studying the impact of NCG in the plant operation and considered the possibility of partial condensation in the tubes bundles. They also took into account the accumulation of steam, seawater around the tubes bundles and brine at the bottom of the effect. Most importantly, they completely redefined the interconnection between the effects by expressing the steam and brine mass flow rates as functions of pressure drops and brine levels between two successive effects. Although this work was very promising, there were some restricting assumptions that led to a limitation regarding the information that could be obtained from the simulations. To address those major issues, we propose a new and more complete version of this model, which is more representative of how real MED plants are operated.

PRE-PRINT of the paper published on Desalination 452 (2019). Note that it may differ from the final published version (https://doi.org/10.1016/j.desal.2018.10.026) due to several revisions implemented during the peer review process of the journal.

This paper is organized as follows:
- in the second section, the MED-TVC Trapani plant is described;
- in the third section, the new proposed dynamic model is described, highlighting all the improvements with respect to the previous version;
- in the fourth section, a steady state validation of the model is presented based on experimental data obtained from the MED-TVC plant operated in Trapani (Sicily);
- in the fifth section, transient simulations are presented considering much wider range of possible disturbances and demonstrating flexibility and criticalities of transient operation of a MED plant, eventually leading to the definition of a control strategy for a MED plant.
- finally, a conclusion is given in the sixth section.

2. Description of the MED-TVC Trapani plant

The model proposed here is based on the features of the desalination plant located in Trapani (Italy). This multiple-effect distillation plant is composed of four parallel and identical MED units equipped with a thermal vapour compressor. Each unit comprises a twelve effects cascade and produces 9000 m^3/d of desalinated water, thus the total capacity of the plant is 36 000 m^3/d. There are approximately 11,000 horizontal tubes in each effect, placed in a 4.8 m diameter shell.
Thanks to the combination of vapour compression and MED plant features, the Gain Output Ratio (GOR) is very high: almost 17 tons of water are produced for 1 ton of motive steam. In each unit, 5 preheaters, one every two effects, are used to preheat the incoming seawater, so that it enters the effects at a temperature as close as possible to the saturation one. The motive steam supplied to the ejectors - for thermo-compression and air venting - is produced in two methane boilers, each one generating up to 60 t/h of saturated steam at 45 bars It is worth mentioning that part of the condensate produced in the first effect is recycled to feed the methane boilers. As can be seen on the sketch of one unit in Fig.1, an extraction system for non-condensable gases from the final condenser is also integrated. Non-condensable gases present in one effect are entrained to the next effects, the preheaters and are then extracted from the final condenser. For confidentiality issues, some geometrical and heat transfer properties concerning this process are not given. More information on the operating data, layout and history can be found in [4,19,20].

PRE-PRINT of the paper published on Desalination 452 (2019). Note that it may differ from the final published version (https://doi.org/10.1016/j.desal.2018.10.026) due to several revisions implemented during the peer review process of the journal.

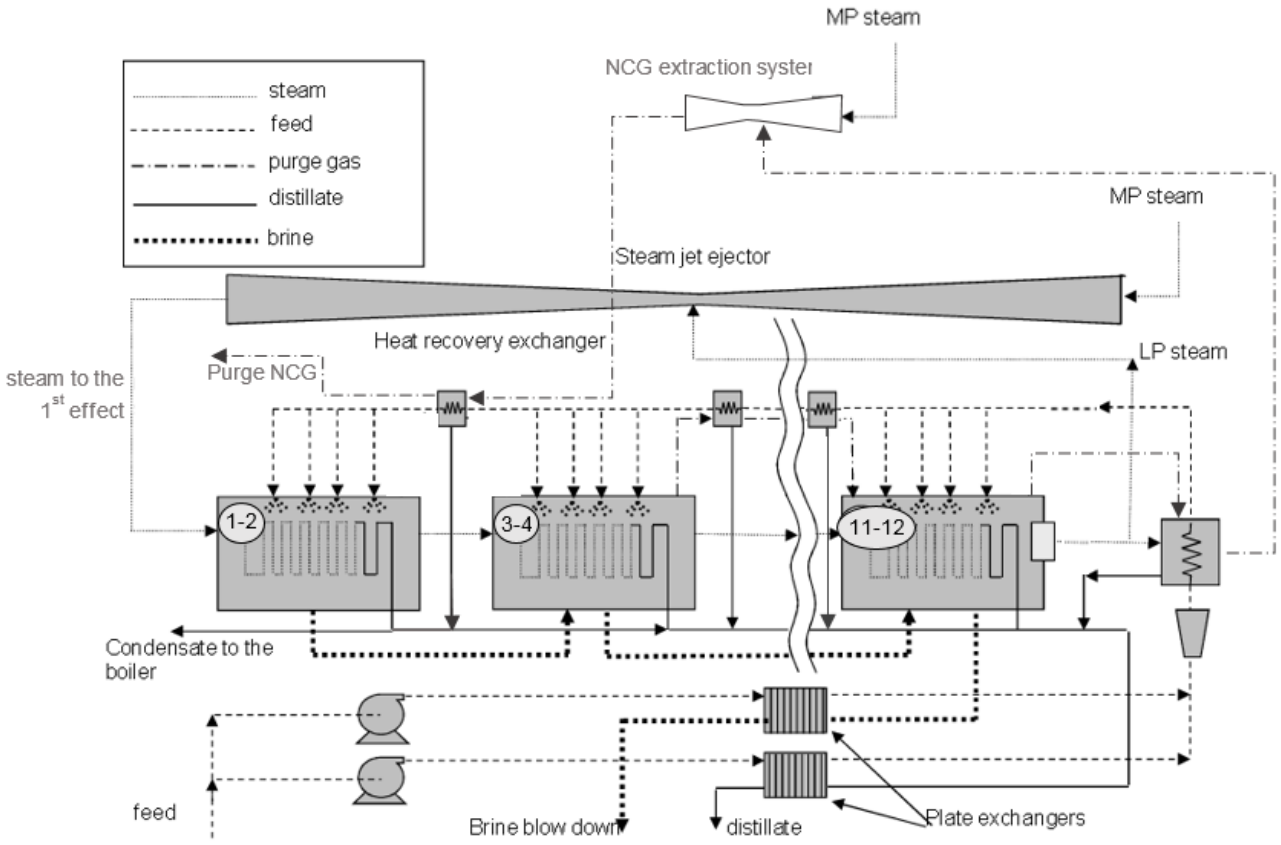

Fig.1. Simplified sketch of the MED-TVC plant in Trapani. Source: adapted from [4,19]

3. Dynamic model description

3.1 Global structure and main hypothesis

The following model is partly based on the model developed by Cipollina *et al* in [4]. Several improvements are proposed to make the model more representative of the real MED plant operation and to describe more accurately the transient behaviour of the MED-TVC plant. Therefore, the main hypothesis and the global structure of the model are similar to the previous work:

- The produced steam is free of salts;
- The vapor phase containing steam and non-condensable components is assumed to be an ideal gas;
- No thermal losses through the walls are considered;
- Evaporation chambers are assumed to be perfectly sealed so that the only source of NCG species is due to the outgassing of seawater;
- To ensure that saturated steam feeds the 1st effect after the steam ejector, a distillate flow rate of 1 kg/s (value taken from the nominal plant operation data) is recycled from the first effect's condensate and mixed to the motive steam. This process is considered in the model;
- The physical properties are calculated by using constitutive equations, mostly developed by El-Dessouky *et al.* [5].

PRE-PRINT of the paper published on Desalination 452 (2019). Note that it may differ from the final published version (https://doi.org/10.1016/j.desal.2018.10.026) due to several revisions implemented during the peer review process of the journal.

- The other components: steam ejector, pre-heaters and final condenser are modelled using steady-state equations. Indeed, mainly due to the lack of information on the pre-heaters and final condenser geometry they can not be modelled with dynamic equations. Furthermore, as will be explained later, the ejector's dynamic is the reason why it is described with stationary equations.

The initial model performed quite well but has several restricting assumptions. This led to a limitation regarding the dynamic analysis of the MED-TVC plant. Some of those assumptions were mentioned in the previous work, to highlight the fact that more work was needed to be done for a better understanding of the plant behaviour under transient conditions.
First of all, some of the NCG equations had to be corrected. Indeed, the solubility of the NCG species in the seawater was wrongly calculated and additional information was needed for clarification purposes.
Secondly, the pre-heaters needed to be accurately modelled – even in steady-state – because the feed seawater temperature in the effects has a great impact on the effect variables. In the previous work, the exiting seawater temperature at each pre-heater was fixed for all the simulations, which is a huge limitation regarding the dynamic analysis of the plant's behaviour.
Thirdly, as can be shown in [16], during the heat transfer between the condensation and evaporation processes, heat is accumulated in the tubes' wall and this has an influence on the performances as not all the latent heat is available for evaporating the seawater in the effect. Therefore, it is major to implement dynamic equations for the characterisation of the heat transfer. In addition, for modelling the effect accurately in dynamic conditions, it is not correct to use steady-state equations directly combined with dynamic ones.
Finally, and most important of all, the brine connection between two successive effects has a huge impact on the stability of the plant and they have to be implemented in the model as well as every other component.
All those considerations were the motivations of the current work and with those taken into account, for a better description of the physical phenomenon, we now have a complete model that allows us to study the potential of operating a MED plant under dynamic conditions.
Two simulation platforms were used to implement the model described in this article. The first is the equation-based process simulator gPROMS®, which allows the use of a hierarchical model structure with three hierarchical levels: lower level (effect *i*), middle level (n effects, preheaters, steam ejector, final condenser) and higher level (MED-TVC plant) and the second platform is MATLAB®. This led to re-writing the model to develop one mathematical structure that can handle globally this problem.
In order to derive a unique global numerical solution representing all the variables, we define a state vector – for each effect – $X_{mat}{}^{T} = [Vap\ B_{pool}\ B_{shell}\ x_{shell}\ x_{pool}\ Y_{vap}\ X_{shell}\ X_{pool}\ T_{vap}\ T_{shell}\ T_{pool}\ T_{w}]$ and a matrix A_{mat} such as $\frac{dX_{mat}}{dt} = A_{mat}$. All the differential equations for each effect are solved simultaneously, using the solver ode15s, asit solves stiff differential equations and DAEs with a variable order method so it was the most adequate one.
All the results presented in this article are from MATLAB® but they were thoroughly compared to the ones obtained from gPROMS® - for the same model equations - to ensure that there were no mistakes made in the implementation or due to the use of different solvers.

3.2 Basic structure of the model

3.2.1. Effect model

PRE-PRINT of the paper published on Desalination 452 (2019). Note that it may differ from the final published version (https://doi.org/10.1016/j.desal.2018.10.026) due to several revisions implemented during the peer review process of the journal.

As represented in Fig.2, an effect is described by three phases, the properties of each phase being assumed to be uniform. Consequently, the state of the flows leaving an effect is the same as the one inside the effect:

- the vapour phase I is a mixture of water and NCG species;
- the phase II is the dispersed brine around the tube bundle;
- the phase III is the brine pool liquid.

Each phase is described by differential equations for mass, energy, non-condensable species and salts conservations.

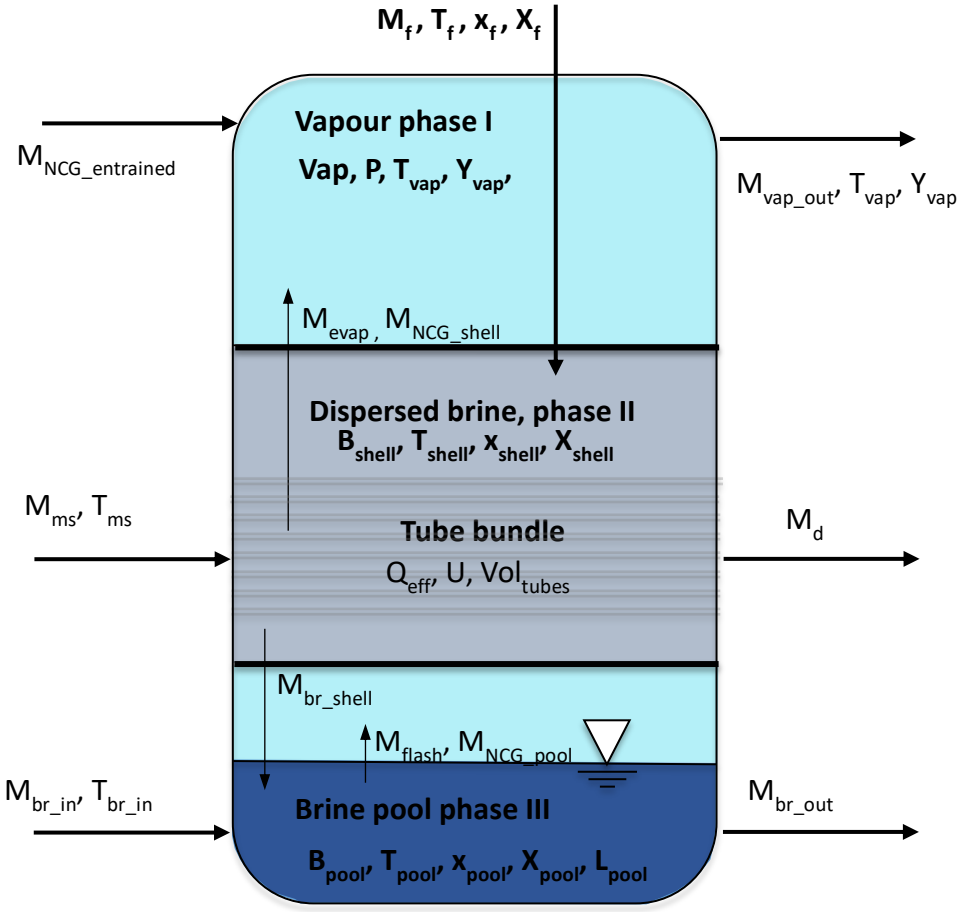

Fig. 2. One effect simplified representation. Source: adapted from [4].

Equations (1), (2) and (3) represent the total mass conservation in each phase:

$$\frac{dVap}{dt} = M_{evap} - M_{vap\_out} + M_{flash} + M_{NCG\_shell} + M_{NCG\_entrained} + M_{NCG\_pool} \quad (1)$$

$$\frac{dB_{shell}}{dt} = M_f - M_{evap} - M_{br\_shell} - M_{NCG\_shell} \quad (2)$$

$$\frac{dB_{pool}}{dt} = M_{br\_shell} + M_{br\_in} - M_{br\_out} - M_{flash} - M_{NCG\_pool} \quad (3)$$

M stands for mass flow rates. The vapour phase I is fed by the evaporation of seawater (M_{evap}) from the sprayed tubes, the flashed vapour from the brine coming from the previous effect (M_{flash} is defined

in part 3.3.2.1) and the NCG species flow-rates (M_{NCG}) coming from the two other phases and entrained from the previous effect. The phase II, which corresponds to the retention of seawater around the tube bundle, is fed by seawater entering the effect (M_f), while the evaporated vapour mass flow rate (M_{evap}) flows to phase I, the released NCG species (M_{NCG_shell}) and the mass flow rate of seawater (M_{br_shell}) leave the tube bundle (phase II). Regarding phase III, the brine pool mass variation is directly linked to the amount of brine entering (M_{br_in}) and exiting the effect (M_{br_out}), the seawater coming from phase II, the quantity of flashed vapour and released NCG species (M_{NCG_pool}).
Some of the effects are connected to a pre-heater, therefore part of the vapour produced inside flows into the pre-heater and the remaining part flows toward the next effect. The term M_{vap_out} is corrected by the amount of vapour that goes into the pre-heater, when there is one.

Since time variations of pressure are neglected, the energy balance equations for phases I and III can be obtained from equations (1) and (3), each term being multiplied by the corresponding specific enthalpy.

As far as phase II is concerned, an additional term, Q_{eff}, has to be included, as is displayed in equation (4).

$$\frac{d(B_{shell} \,.\, h_{shell})}{dt} = M_f \cdot h_f + Q_{eff} - M_{evap} \cdot h_{evap} - M_{br\_shell} \cdot h_{shell} - M_{NCG\_shell} \cdot h_{NCG\_shell} \quad (4)$$

Q_{eff} is the heat flux transferred through the tube bundle from the condensing steam, whose expression will be detailed later in this paper as it is one of the main improvements made in the model. As the three phases are not in equilibrium conditions, heat fluxes between phases exist but have been neglected.
T As equation (5) relates the temperature to the associated specific enthalpy, the temperature in each phase can be obtained by combining equations (4) and (5).

$$\frac{dh_{phase}}{dt} = Cp_{phase} \cdot \frac{dT_{phase}}{dt} \quad (5)$$

Some additional equations (6), (7), (8) and (9) are necessary to implement this model.

$$P = \frac{Vap \cdot R \cdot T_{vap}}{PM_{H2O} \cdot Vol_{vap}} \quad (6)$$

Equation (6) gives the pressure inside one effect, depending on the vapour temperature and the amount of NCG species, as we considered the vapour phase as an ideal gas.

$$Mass_{phase} = Vol_{phase} \cdot \rho_{phase} \quad (7)$$

$$Vol_{pool} = L_{SE} \cdot \left(\frac{D_{SE}^2}{4} \cdot \arccos \frac{D_{SE}/2 - L_{pool}}{D_{SE}/2} - (D_{SE}/2 - L_{pool}) \cdot \sqrt{L_{pool} \cdot (D_{SE} - L_{pool})} \right) \quad (8)$$

$$Vol_{SE} = Vol_{vap} + Vol_{pool} + Vol_{tubes} + Vol_{shell} \quad (9)$$

PRE-PRINT of the paper published on Desalination 452 (2019). Note that it may differ from the final published version (https://doi.org/10.1016/j.desal.2018.10.026) due to several revisions implemented during the peer review process of the journal.

Equations (8) is relating the brine pool level with the associated volume in a horizontal cylinder. Equation (9) needs to be true at each moment of the simulation. The volume of the liquid dispersed around the tube bundle (Vol_{shell}), was estimated by assuming an uniform mean film thickness around each tube with a fixed thickness of 0.5 mm [18].

The equations (10) and (11) for the mass conservation of salts in each liquid phase are expressed below.

$$\frac{dS_{shell}}{dt} = M_f \cdot x_f - M_{br\_shell} \cdot x_{shell} \quad (10)$$

$$\frac{dS_{pool}}{dt} = M_{br\_shell} \cdot x_{shell} + M_{br\_in} \cdot x_{br\_in} - M_{br\_out} \cdot x_{pool} \quad (11)$$

S stands for the total mass of salts and x is for the salt mass fraction. For each phase they are related by equation (12).

$$S_{phase} = B_{phase} \cdot x_{phase} \quad (12)$$

As mentioned before, non-condensable species must be considered in the equations as they can strongly influence the steady state and dynamic behaviour of the plant. They are considered as one single species according to the mass balance differential equations (13), (14) and (15) for each phase:

$$\frac{dNCG_{vap}}{dt} = M_{NCG\_shell} + M_{NCG\_entrained} + M_{NCG\_pool} - M_{vap\_out} \cdot Y_{vap} \quad (13)$$

$$\frac{dNCG_{shell}}{dt} = M_f \cdot X_f - M_{NCG\_shell} - M_{br\_shell} \cdot X_{shell} \quad (14)$$

$$\frac{dNCG_{pool}}{dt} = M_{br\_in} \cdot X_{br\_in} + M_{br\_shell} \cdot X_{shell} - M_{br\_out} \cdot X_{pool} - M_{NCG\_pool} \quad (15)$$

NCG_{phase} is for the total mass of NCG in the considered phase and Y_{vap} and X_{phase} stands for the NCG species mass fraction in gas and liquid phase respectively, they are both linked with the mass of vapour or liquid in the phase by equation (16) and (17), respectively.

$$NCG_{vap} = Vap \cdot Y_{vap} \quad (16)$$

$$NCG_{phase} = B_{phase} \cdot X_{phase} \quad (17)$$

NCG species are released only if their concentration in the liquid is superior to the equilibrium solubility of NCG. In this system configuration, we consider only the situation when the NCG flux comes from the liquid phase to the vapour phase. This is what the equation (18) represents.

$$M_{NCG\_phase} = M_{phase\_in} \cdot (X_{phase} - X_{phase\_eq}) \cdot \theta \quad (18)$$

The NCG transfer mass flux is represented by a fraction θ accounting for the uncomplete striping of the NCG species. Due to the lack of information about the phenomenon of non-complete stripping of the NCG from the liquid, it has been assumed that it has the same weight as the NEA temperature drop due to the brine flashing. The value of 0.75 is chosen in analogy with the previous work [4] and

is constant in all simulations. X_{phase_eq} stands for the solubility of the NCG species in a liquid phase at equilibrium with the vapor phase and is calculated by using equations (19) and (20) that are obtained as follows.

We limit the analysis to the consideration of O_2 and N_2 as NCG species. Indeed they represent the greatest proportion of NCG species which are molecularly dissolved and do not react chemically in seawater nor are produced during the desalination process itself [21]. Outgassing of CO2 is out of the scope of this analysis as it reacts chemically with carbonates in seawater and it requires additional equations other than only considering the solubility of the different species.
The solubility of O_2 and N_2 as NCG species are given by equilibrium conditions [22], as shown in equations (19) and (20), where $H_{c\_O2}(T,X_b)$ and $H_{c\_N2}(T,X_b)$ are the Henry coefficients depending on the temperature and the salt composition .

$$Y_{mol\_O2} \cdot P = H_{c\_O2}(T,X_b) \cdot X_{mol\_eq\_O2} \quad (19)$$
$$Y_{mol\_N2} \cdot P = H_{c\_N2}(T,X_b) \cdot X_{mol\_eq\_N2} \quad (20)$$

In the equations, NCG species are considered as one component. Therefore, equations (19) and (20) have to be added to each other in order to define a mean value of the Henry coefficients as follows in equation (21)

$$(Y_{mol\_O2}+Y_{mol\_N2}) \cdot P = H_c(T,X_b) \cdot (X_{mol\_eq\_O2} + X_{mol\_eq\_N2}) \quad (21)$$

With H_c defined as shown in equation (22)

$$H_c = \frac{H_{c\_O2} + H_{c\_N2}}{2} \quad (22)$$

This is only possible because the Henry coefficients of the two species are close enough.

In order to calculate the Henry coefficients $H_{c\_O2}(T,X_b)$ and $H_{c\_N2}(T,X_b)$, we have used the available solubility data of O_2 and N_2 in seawater in contact with ambient air, as given by the correlation (23) where T is in Kelvin and C_G in µmol/kg [23] (see Table 1).

$$C_G = \exp\left[A_1+A_2\left(\frac{100}{T}\right)+A_3\ln\left(\frac{T}{100}\right)+A_4\left(\frac{T}{100}\right)+\frac{X_B}{1000}\left(B_1+B_2\frac{T}{100}+B_3\left(\frac{T}{100}\right)^2\right)\right] \quad (23)$$

Table 1 . Constants for estimating gas solubility in seawater [23] **in contact with ambient air**

	A_1	A_2	A_3	A_4	B_1	B_2	B_3
O_2	-172.9894	255.5907	146.4813	-22.2040	-0.037362	0.016504	-0.0020564
N_2	-173.2221	254.6078	146.3611	-22.0933	-0.054052	0.027266	-0.0038430

PRE-PRINT of the paper published on Desalination 452 (2019). Note that it may differ from the final published version (https://doi.org/10.1016/j.desal.2018.10.026) due to several revisions implemented during the peer review process of the journal.

By applying equilibrium conditions (19) and (20) to the solubility data as given by correlation (23), one can easily find the expression of the Henry coefficients. In those conditions, $Y_{mol\_O2} = 0.21$ and $Y_{mol\_N2} = 0.78$, the pressure is the atmospheric pressure:

$$Y_{mol\_O2} \cdot P_{atm} = H_{c\_O2} \cdot C_{G\_O2} \cdot PM_{sw} \quad (24)$$

$$Y_{mol\_N2} \cdot P_{atm} = H_{c\_N2} \cdot C_{G\_N2} \cdot PM_{sw} \quad (25)$$

where C_G is expressed in mol/kg. $PM_{sw} = 18.43.10^{-3}$ kg/mol is the seawater molar weight based on the seawater composition: 96.5% of water and 3.5% of salts. Salts are composed of: 55% of chloride, 30.6% of sodium and 7.7% of sulfates.

3.2.2. Vapour flow rates between effects

The expression of the mass flow rate of vapour exiting one effect, thus entering the condensation zone of the next effect with the same thermodynamic properties, is similar to the one for the brine and is described by equation (26).

$$M_{vap\_out}(i) = \alpha(i) \cdot \sqrt{\rho_{vap}(i) \cdot (P(i) - P(i+1))} \quad (26)$$

The mass flow rate is also a function of the pressure difference between two successive effects and a discharge coefficient α.

The stream of vapour exiting the 12th effect is divided into two parts, one part is entrained by the steam ejector and the remaining part goes to the final condenser.

3.2.3. Final condenser model

The final condenser is an important component of the process as it condenses part of the vapour produced in the last effect that is not fed to the steam ejector. In addition, it also increases the intake seawater temperature before it is sprayed across the effects 11 and 12. NCG flowing through the venting lines also reach the final condenser where they are extracted by the NCG ejector.

The final condenser is modelled with stationary equations (27) to (30).

$$Q_{cond} = M_{vap\_out}(12) \cdot \left(1 - Y_{vap}(12)\right) \cdot \lambda_{vap}(12) \quad (27)$$

$$Q_{cond} = M_{sw\_in} \cdot C_{p_{sw\_in}} \cdot \left(T_{sw\_out} - T_{sw\_in}\right) \quad (28)$$

$$Q_{cond} = U_{cond} \cdot A_{cond} \cdot LMTD \cdot \left(1 - Y_{vap}(12)\right) \quad (29)$$

$$LMTD = \frac{\left(T_{vap} - T_{sw\_in}\right) - \left(T_{vap} - T_{sw\_out}\right)}{\ln\left(\frac{T_{vap} - T_{sw\_in}}{T_{vap} - T_{sw\_out}}\right)} \quad (30)$$

In equation (27), the term $M_{vap\_out}(12) \cdot \left(1 - Y_{vap}(12)\right)$ expresses the steam flow rate in the mixture of steam and NCG.

PRE-PRINT of the paper published on Desalination 452 (2019). Note that it may differ from the final published version (https://doi.org/10.1016/j.desal.2018.10.026) due to several revisions implemented during the peer review process of the journal.

The equation (28) represents the enthalpy variation of the intake seawater, so that it is possible to deduce the temperature of the exiting seawater that will go into the first preheater or will be sprayed into the effects 11 and 12.
The equation (29) is the heat flux between condensing vapour and evaporating seawater, in which the term $\left(1-Y_{vap}(12)\right)$ is included to estimate its reduction due to the NCG, LMTD is the logarithmic mean temperature difference and U_{cond} is the overall heat transfer coefficient that is calculated by using a correlation developed by El-Dessouky *et al.* [5], as described in appendix I.
For confidentiality reasons, information on the condenser heat transfer area and geometry cannot be disclosed.

3.2.4. Steam ejector model

A steam ejector improves the performances of a MED plant. Part of the vapour produced in the last effect is compressed with high-pressure motive steam (45 bars) to generate the heating steam fed into the first effect.
The steam ejector can be divided into four parts: the nozzle, where the motive steam enters, the suction chamber, the throat and the diffuser. The suction chamber and the diffuser are converging/diverging Venturi tubes.
As the response of the steam ejector is much faster than the one of the desalination unit, a stationary model was implemented and is detailed in appendix II.

The mathematical model was developed by El-Dessouky *et al.* [9]. It allows calculating the pressure profiles along the different areas along with the associated Mach numbers. The pressure of the motive and entrained steam are the sole inputs of the model. The outputs are the mass flow rates of entrained and motive steam and the pressure and mass flow rate of the compressed steam that will then enter the condensation zone of the first effect.
Furthermore, the model accounts for geometrical and physical parameters. Thus it was initially used in a reverse algorithm using operation data as entries for the model, as described in [9], to determine the geometric parameters. Once the geometry of the ejector along with other parameters were set, the model could then be used for performance predicting purposes.
The predicted results were compared against operation data and the model was validated with a good fitting, as shown in section 4.

3.2.5. Total distillate production

This variable is one of the most important ones to describe the plant performances. It is detailed in equation (31).

$$D_{tot} = \sum_{i=1}^{13} M_d(i) + \sum_{j=2}^{5} M_{ph}(j) - M_p - M_{ds} \quad (31)$$

$M_d(i)$ is the distillate produced in effect i and in the final condenser, $M_{ph}(j)$ stands for the amounts of vapour condensed in the preheaters whose description will be detailed later and M_{ds} is the condensed vapour part fed to the de-super-heater. Finally, M_p is the fraction of the distillate from the 1st effect that returns to the boilers to produce the ejector high-pressure steam.

3.2.6. Gain output ratio (GOR)

PRE-PRINT of the paper published on Desalination 452 (2019). Note that it may differ from the final published version (https://doi.org/10.1016/j.desal.2018.10.026) due to several revisions implemented during the peer review process of the journal.

The GOR is the ratio between the total distillate mass flow rate and the motive high-pressure steam required at the steam ejector, as shown in equation (32).

$$GOR = \frac{D_{tot}}{M_p} \tag{32}$$

3.3 New considerations for the MED-TVC dynamic model

3.3.1 Condensation and evaporation processes modelling

Initially, the evapo-condenser heat exchangers were modelled in steady-state by using a global heat transfer coefficient. Due to the thermal inertia of these heat exchangers, a more accurate way to describe such phenomena is to differentiate the evaporation from the condensation fluxes and to account for the energy accumulated inside the tubes material with the dynamic enthalpy balance equation (33).

$$Vol_{tubes} \cdot \rho_{tubes} \cdot Cp_{tubes} \cdot \frac{dT_w}{dt} = Q_{eff\_cond} - Q_{eff} \tag{33}$$

The equation (33) is used to link the evaporation and condensation fluxes that are calculated as follows. As the alloy of the tube has a high thermal conductivity and the thickness of the tube is small, the conduction across the tube can be neglected. Therefore, the temperature is assumed to be uniform in the whole tube bundle.

Partial condensation in the tube bundle is considered by equations (34) to (38). ε is the ratio between the energy available from the total condensation of the incoming vapour mass flow rate and the available heat transfer rate. As we assumed that NCG species do not enter the condensing area, $M_{ms} \cdot (1-Y_{ms})$ represents the fraction of steam in the incoming vapour.

$$\varepsilon = \frac{M_{ms} \cdot \lambda_{ms} \cdot (1 - Y_{ms})}{U_{cond} \cdot A_{cond} \cdot (T_{cond} - T_w)} \tag{34}$$

Case 1: ε <= 1: the heat transfer rate is superior to the one requested for the total condensation of the incoming steam, thus the heat transfer rate will then be based on the condensation heat only.

$$Q_{eff\_cond} = M_{ms} \cdot \lambda_{ms} \cdot (1 - Y_{ms}) \tag{35}$$
$$M_d = M_{ms} \cdot (1 - Y_{ms}) \tag{36}$$

Case 2: ε > 1: as the transfer rate is lower than the one required for the condensation of the incoming steam, partial condensation occurs, and the distillate mass flow must be corrected

PRE-PRINT of the paper published on Desalination 452 (2019). Note that it may differ from the final published version (https://doi.org/10.1016/j.desal.2018.10.026) due to several revisions implemented during the peer review process of the journal.

$$Q_{eff\_cond} = U_{cond} \cdot A_{cond} \cdot (T_{cond} - T_w) \quad (37)$$

$$M_d = \frac{U_{cond} \cdot A_{cond} \cdot (T_{cond} - T_w)}{\lambda_{ms}} \quad (38)$$

The heat transfer coefficient for the condensation process U_{cond} inside the tube bundle is calculated by the equation developed by Chato [24] for predicting gravity-dominated condensation on the basis of the Nusselt analysis (see appendix I).

The evaporation flux is given by equation (39) and it is also the definition of Q_{eff} that was previously mentioned in equation (4) and (33).

$$Q_{eff} = A_{shell} \cdot U_{shell} \cdot (T_w - T_{shell}) \quad (39)$$

In a falling film evaporator, the liquid is sprayed across the horizontal tube bundle, so that part of it evaporates while the remaining part flows over the tubes below. Several correlations based on the Nusselt number have been published [25] and are easily usable for the description of a falling film evaporator without calculating the thickness of the seawater film around the tubes. The correlation used here was developed by Sernas [26] and is described in equations (41) to (44).

$$Nu = \frac{U_{shell}}{k_{shell}} \cdot \left(\frac{\mu_{shell}^2}{g \cdot \rho_{shell}^2}\right)^{1/3} \quad (40)$$

$$Nu = 0.041 \cdot Re^{0.3} \cdot Pr \cdot Ar^{-0.04} \quad (41)$$

$$Re = \frac{4 \cdot \Gamma}{\mu} \quad (42)$$

$$Pr = \frac{\nu}{k} \quad (43)$$

$$Ar = \frac{D_{tubes\_ext}^3 \cdot g}{\nu_{shell}^3} \quad (44)$$

3.3.2 Brine pipes modelling

3.3.2.1 Flash of the incoming brine

The additional amount of vapour produced by the isenthalpic flashing of the incoming brine is depicted by equation (45). It is assumed that the brines flashes in steady-state conditions, prior to its arrival into the effect I, and that the produced vapour feeds the vapour phase I and the remaining brine feeds phase III.

From the mass conservation law, equations (46) to (48) are used to determine the brine mass flow rate arriving in the pool phase and its temperature and salinity.

$$M_{br\_out}(i-1) \cdot Cp_{br\_in}(i) \cdot \left(T_{pool}(i\text{-}1) - (T_{vap}(i) + BPE(i) + NEA(i))\right) = M_{flash}(i) \cdot \lambda_{vap}(i) \quad (45)$$

$$M_{br\_in}(i) = M_{br\_out}(i-1) - M_{flash}(i) \quad (46)$$

$$M_{br\_out}(i-1) \cdot x_{br\_out}(i-1) = M_{br\_in}(i) \cdot x_{br\_in}(i) \quad (47)$$

$$T_{br\_in} = T_{vap}(i) + BPE(i) + NEA(i) \quad (48)$$

PRE-PRINT of the paper published on Desalination 452 (2019). Note that it may differ from the final published version (https://doi.org/10.1016/j.desal.2018.10.026) due to several revisions implemented during the peer review process of the journal.

The exiting brine flow from the previous effect is divided between the flashed vapour flow, salt free, and the liquid flow feeding the phase III. The correlation for the boiling point elevation (BPE) and the non-equilibrium allowance (NEA) are given in appendix 1.

3.3.2.2 U- pipes

The brine pool level inside the effects has a very slow dynamic in comparison to other variables, like the temperature, which make them the hardest parameter to control when operating a MED plant. Indeed, a small variation in the incoming vapour pressure can lead to great instabilities regarding the level. The major problem is that there is a small range for the possible level, very often under 0 m the effect is considered as empty and above 0.6 m the effect can be considered flooded as it reaches the first row of tubes bundles. The average level height is 0.3 m, so there is not a high flexibility during the operation of the MED plant. Which is the reason why it is highly important to describe as well as possible the phenomenon affecting the brine pool level.
Furthermore, as it was mentioned in [4], even if no information can be found in the literature about the control systems adopted for regulating the brine pool level in the effects, it is well known that the use of U-pipes, Fig.3, for connecting two successive effects can significantly help to regulate the brine flow and the level. Such U-pipes are used in the Trapani plant and a model must be proposed to represent the brine connection between two effects since the brine pool level variations are very hard to manage.

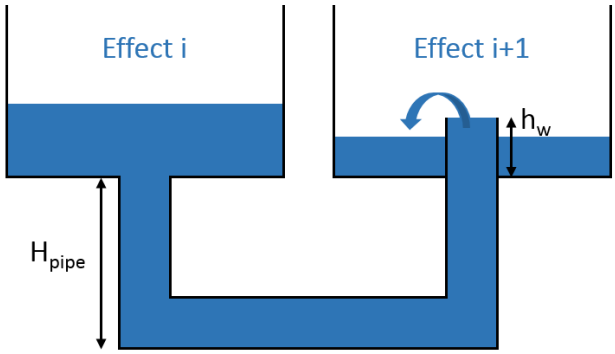

Fig. 3. Sketch of a U-pipe connecting the brine pools between two successive effects.

As shown in Fig.3, the U-pipe allows the brine level to go much below 0 meters, which can lead to a huge gain regarding the stability of the MED plant. For example, in the Trapani plant, the U-pipe height, H_{pipe}, is between 1 and 2 meters. When the level, L_{pool}, is in the vertical part of the U-pipe, it is negative as shown by equation (49).
The equations (49) to (53) describe how to consider this volume and to accurately calculate the level of the brine pool. With these new implementation, two scenarios are possible. If the brine is only in the vertical part of the U-pipe, and not at all inside the effect, then the level is considered as negative and is calculated by equation (52). The second scenario is if the brine is inside the effect, therefore the level is positive and is deduced by equation (53).

$$H_{pipe} < 0 \quad (49)$$
$$H_{pipe} < L_{pool} < 0.6 \quad (50)$$
$$V_{pipe} = A_{pipe} \cdot |H_{pipe}| \quad (51)$$

PRE-PRINT of the paper published on Desalination 452 (2019). Note that it may differ from the final published version (https://doi.org/10.1016/j.desal.2018.10.026) due to several revisions implemented during the peer review process of the journal.

Case 1: ($Vol_{pool} < V_{pipe}$)

$$Vol_{pool} = (|H_{pipe}| + L_{pool}) \cdot A_{pipe} \quad (52)$$

Case 2: ($Vol_{pool} > V_{pipe}$)

$$Vol_{pool} = L_{SE} \cdot \left(\frac{D_{SE}^2}{4} \cdot \arccos \frac{D_{SE}/2 - L_{pool}}{D_{SE}/2} - (D_{SE}/2 - L_{pool}) \cdot \sqrt{L_{pool} \cdot (D_{SE} - L_{pool})} \right) + V_{pipe} \quad (53)$$

Another parameter that leads to enhance the stability is the shape of U-pipe outlet. As shown in Fig.3, there is a weir height, h_w, that must be considered for the expression of the mass flow rate exiting the effect i, as represented by equations (54) to (56).

Case 1: $L_{pool}(i+1) > h_w$

$$M_{br\_out}(i) = Cd_{pool}(i) \cdot A_{pipe}(i) \cdot \sqrt{\left[(P(i) - P(i+1)) + (L_{pool}(i) - L_{pool}(i+1)) \cdot g \cdot \rho_{pool} \right] \cdot \rho_{pool}} \quad (54)$$

Case 2: $L_{pool}(i+1) < h_w$

Case 2.1: $\left((P(i) - P(i+1)) + (L_{pool}(i) - h_w) \right) < 0$

$$M_{br\_out}(i) = 0 \quad (55)$$

Case 2.2: $\left((P(i) - P(i+1)) + (L_{pool}(i) - h_w) \right) > 0$

$$M_{br\_out}(i) = Cd_{pool}(i) \cdot A_{pipe}(i) \cdot \sqrt{\left[(P(i) - P(i+1)) + (L_{pool}(i) - h_w) \cdot g \cdot \rho_{pool} \right] \cdot \rho_{pool}} \quad (56)$$

The equation (54) is used when the level in the effect i+1 is higher than the weir height (around 0.2 meter). Otherwise, the equations (55) and (56) are used. When the brine level in the effect i is below 0 (left branch in Fig.3) and the level in the effect i+1 is below the weir height, this generates a negative ΔL_{pool} value that counteracts the positive ΔP, and it can lead to a negative driving force if ΔL_{pool} is high enough. In this case, the incoming brine cannot reach the effect i+1 and the value of the exiting mass flow rate set to 0. It is worth mentioning that if the incoming brine mass flow rate is set to zero, the brine level in the effect i will increase until the driving force is again positive and the exiting brine mass flow rate greater than zero. The presence of U-pipes and weir heights also help to hydraulically disconnect the effects, giving a much larger allowance for brine level variations.
The mass flow rate of the brine, in equation (56) depends on the pressure difference as well as the difference of the brine pool level between two consecutives effects. A_{pipe} stands for the cross section of the brine pipe.

The equations (54) to (56) are used for the effects 1 to 11. Indeed, at the last effect, the brine is extracted by a pump in order to control the level in the effect. Thus, equation (57) is used for the brine mass flow rate exiting the 12^{th} effect.

PRE-PRINT of the paper published on Desalination 452 (2019). Note that it may differ from the final published version (https://doi.org/10.1016/j.desal.2018.10.026) due to several revisions implemented during the peer review process of the journal.

$$M_{br\_out}(12) = 0.66 \cdot \left(M_{sw\_in} - D_{tot}\right) + G_{pool} \cdot \left(L_{pool}(12) - L_{sp}(12)\right) \quad (57)$$

M_{sw_in} is the mass flow rate of seawater taken at the outlet of the final condenser, D_{tot} is the total amount of distillate produced by the plant, G_{pool} is the controller gain, fixed at 100 kg/(s.m) and L_{sp} is the set-point for the brine pool level, set at 0.3 m. G_{pool} and the coefficient 0.66 were determined after a tuning of the controller.

In the previous article [4], it was explained that due to the lack of levels' control systems, large variation in the plant operating conditions could not be simulated as it led to the end of simulation because the effect is either empty or flooded, thus reducing the information that could be obtained from a transient model. The influence of the new U-pipes model is shown in Fig.4 by representing the 1st effect brine pool level evolution, when increasing the motive steam pressure (to the steam ejector) by 20%. It is clear that the simulation, without the pipe model, was stopped because the effect was seen as empty as the brine level became inferior to 0 m, whereas with these new considerations, the simulation can now run its course and describe a much more stable operation of the MED unit. Therefore, it allows us to perform more simulations with a higher flexibility.

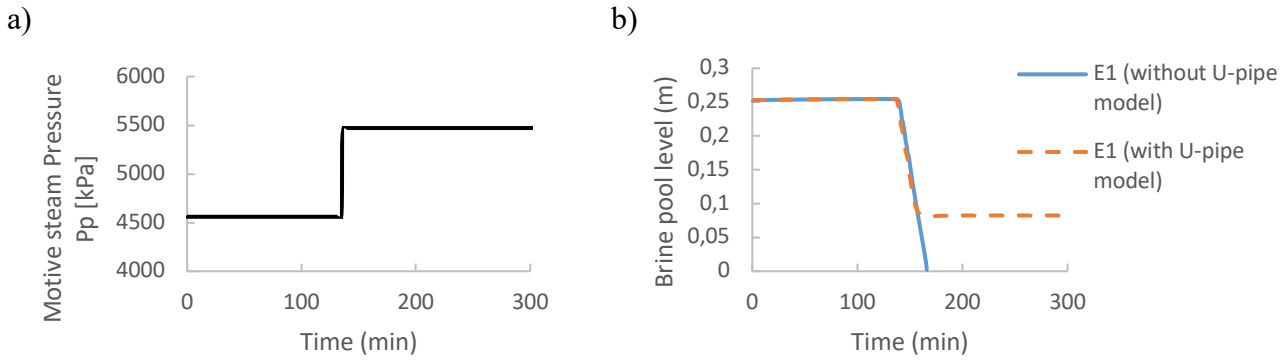

Fig. 4. Response of the system to a step variation of the motive steam pressure by +20%. a) disturbance in Pp; b) brine pool level before and after the implementation of the pipe model.

In the previous article, Cipollina *et al.* [4] tried to study the impact of a step variation of the motive steam pressure by 20%. But no results could be obtained as the U-pipes were not implemented and the emptying of the effect led to the halt of the simulation. With this new implementation, the simulation can now produce results for a step variation greater than +20%, which is a huge improvement.

Moreover, it shows that using U-pipes in MED plants could help significantly in operating the plant as it considerably stabilises the system. Therefore, if a MED plant were to be coupled with renewable energies, it would be crucial to use U-pipes to connect two successive effects.

3.3.3 Pre-heaters model

The seawater flow exiting the final condenser is split into a flow sprayed across the last two effects and a flow going through a cascade of five pre-heaters (one every two effects) feeding the 10 first effects. A mixture of NCG and vapour enters each pre-heater and is condensed therefore providing the energy to be transferred to the incoming seawater. The resulting distillate is then mixed with the

distillate from the previous effect in the distillate duct. It is assumed that all NCG released in one effect go through the pre-heaters until the final condenser where they are extracted by a vacuum ejector.

For the model to be totally representative of the MED-TVC plant operation, there is a need to have the same inputs as the operating control variables, this means the sole inputs have to be the motive steam pressure and the temperature and mass flow rate of seawater entering the final condenser. In the previous version of this model, the temperature of the seawater exiting each pre-heater was fixed according to operating data in nominal conditions, therefore, when the system was simulated under transient conditions, there was a loss of information regarding the dynamic behaviour of each variable.

In this improved version of the model, a steady-state model is assumed for the five pre-heaters allowing calculating the seawater temperature at the effects inlets. Equations (58) to (61) describe the model of the pre-heaters.

$$Q_{ph} = M_{ph} \cdot \lambda_{ph} + (M_{ph} + M_{NCG\_entrained\_ph}) \cdot Cp_{mix} \cdot \Delta T_{vap}(i) \quad (58)$$

$$Q_{ph} = M_{sw\_in\_ph} \cdot Cp_f \cdot (T_{sw\_out\_ph} - T_{sw\_in\_ph}) \quad (59)$$

$$Q_{ph} = U_{ph} \cdot A_{ph} \cdot LMTD_{ph} \quad (60)$$

$$LMTD_{ph} = \frac{(T_{sw\_out\_ph} - T_{sw\_in\_ph})}{\ln\left(\frac{T_{vap} - T_{sw\_in\_ph}}{T_{vap} - T_{sw\_out\_ph}}\right)} \quad (61)$$

These equations allow us to calculate both the incoming vapour mass flow rate and the exiting seawater temperature. U_{ph} is the overall heat transfer coefficient in the pre-heaters and it is calculating by using the same equation as the one used for the heat transfer expression for the final condenser developed by El-Dessouky *et al* [5], (appendix I).

Those new considerations make the whole model more accurate and physically sound. Table 2 shows the comparison between the values that were previously fixed and those obtained from the improved model.

Table 2. Comparison between predicted model values of the temperature of the seawater exiting the pre-heaters with the values that were previously fixed.

	Outlet seawater temperature (°C)					
	Ph 1	Ph 2	Ph 3	Ph 4	Ph 5	Final condenser
Nominal data	55	53.3	48.8	44.2	39.6	34.5
Predicted values	53.8	51.5	47.3	43.2	39.3	35.4

The predicted values are close enough to the operating data to conclude that with these new modifications the reliability of the model in nominal conditions is kept very good. Therefore, with this new implementation, the simulations for off-design conditions are now more accurate.

PRE-PRINT of the paper published on Desalination 452 (2019). Note that it may differ from the final published version (https://doi.org/10.1016/j.desal.2018.10.026) due to several revisions implemented during the peer review process of the journal.

Table 3 shows the comparisons between the results obtained by the fixed temperature model and the improved one in nominal conditions and when the intake seawater temperature is 4°C lower than in nominal conditions.

Table 3. Comparison between the fixed and predicted model temperature: nominal and non-nominal conditions.

	Fixed temperature model [°C]	Calculated temperature model [°C]
T_{sw_in} & M_{sw_in} nominal conditions		
GOR [-]	16.4	16.3
D_{tot} [kg/s]	102.4	101.6
$T_{sw\_out\_ph2}$ [°C]	53.3	51.5
$T_{sw\_out\_ph4}$[°C]	44.2	43.2
-4° C T_{sw_in}		
GOR [-]	16.2	15.3
D_{tot} [kg/s]	101.2	95.5
$T_{sw\_out\_ph2}$ [°C]	53.3	48.8
$T_{sw\_out\_ph4}$ [°C]	44.2	39.5

Table 3 shows that if there is a change in the intake seawater temperature, it cannot be described accurately if the pre-heaters are not well represented.

3.3.4 Additional comparisons with the previous model

In this section, the previous and current models are compared. The simulations performed are the same as in the previous paper [4]. Firstly a perturbation on the motive steam pressure is studied: +10% (Fig.5.a), then one on the intake seawater mass flow rate: -5% (Fig.6.a).
The brine levels are the most critical variables, therefore the comparison is focused on those variations.

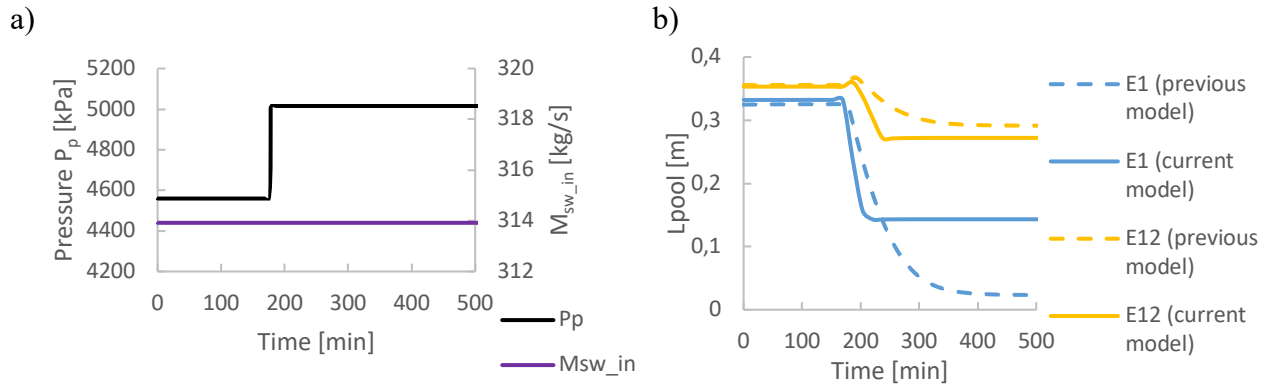

Fig.5: Comparison between the previous and current models for a step variation of the motive steam pressure by +10%. a) Disturbances in the input variables; b) brine pool levels variations

a) b)

PRE-PRINT of the paper published on Desalination 452 (2019). Note that it may differ from the final published version (https://doi.org/10.1016/j.desal.2018.10.026) due to several revisions implemented during the peer review process of the journal.

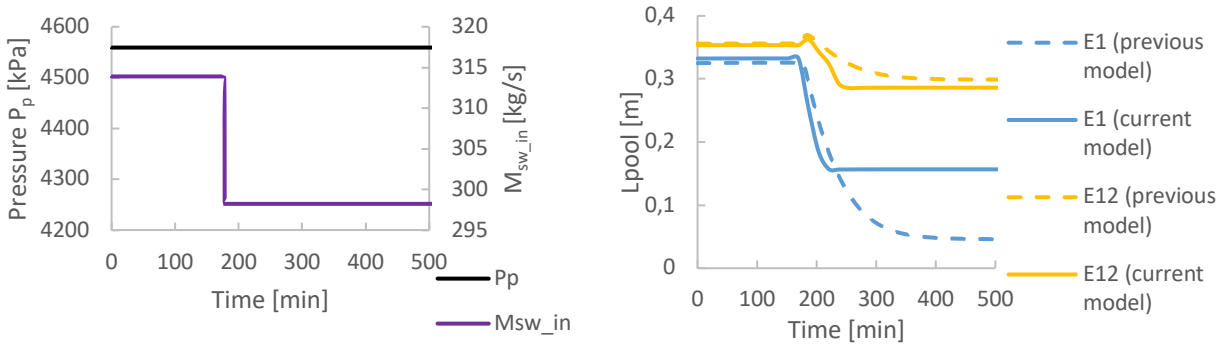

Fig.6: Comparison between the previous and current models for a step variation of the intake seawater mass flow rate by -5%. a) Disturbances in the input variables; b) brine pool levels variations

Both perturbations lead to almost emptying the first effect, in the case of the previous model. With all the new implementations, the current model is now more representative and robust. Indeed as can be seen in Fig.5.b and Fig.6.b, the first effect is, now, far from emptied, which means that it is now possible to run more simulations than before and that the model is now more physically-sound. In addition, with the U-pipes modelling, it is clear that the brine levels dynamics is faster than before, as it takes less time to reach a new steady-state. Finally, when a perturbation occurs in the input parameters, the first effects react more critically than the last ones.

To conclude the whole model description, it is worth reminding that the sole inputs are the motive steam pressure (to the steam ejector) and the intake seawater mass flow rate and temperature at the final condenser. The geometrical parameters for each component were implemented to be representative of the MED-TVC plant in Trapani. This model can calculate every other variable, such as temperature, pressure, NCG concentration, brine level, etc., based on those inputs.
This model is based on mass, energy and salt conservation equations with several correlations to estimate the heat transfer coefficients for the condensation and evaporation processes. Thus, there are 12 differential equations per effect, with multiple additional equations, that are solved simultaneously. The other components, pre-heaters, steam ejector and final condenser, are modelled with steady-state equations.

4. Steady-state calibration and validation of the model

Experimental data for steady-state operations of the Trapani MED plant are available but for confidentiality reasons, it is only possible to compare the model predicted results against some of these nominal operation conditions data.
The values for the coefficient Cd (for the brine) and α (for the vapour) have been obtained by a tuning procedure in order to have a good fitting between the nominal conditions and the results from the model under the same conditions, as shown in Table 4 and 5. More details on the tuning procedure can be found in the previous work [4]

Table 4. Brine discharge coefficient values. Source : [4]

Effect number	1	2	3	4	5	6	7	8	9	10	11
$Cd_{pool}(i)$	0.2756	0.2341	0.2492	0.3823	0.3392	0.4148	0.4785	0.4911	0.5124	0.6551	0.6652

PRE-PRINT of the paper published on Desalination 452 (2019). Note that it may differ from the final published version (https://doi.org/10.1016/j.desal.2018.10.026) due to several revisions implemented during the peer review process of the journal.

[-]											

Table 5. Values of the α coefficients

Effect number	1	2	3	4	5	6	7	8	9	10	11
α(i) [m²]	0.5412	0.6080	0.6859	0.7772	0.7914	0.8807	0.8565	0.9605	0.9942	1.0399	0.8971

The discharge coefficient represent the non-ideal behavior of nozzles in fluid dynamics, and it is defined as the dimensionless ratio of the actual mass flow rate to the ideal mass flow rate corresponding to one-dimensional isentropic flow for the same upstream stagnation conditions. Therefore, it can be considered as constant coefficients within the range of operating conditions considered in this study (independently from dynamic or steady-state operations).

In Table 6 is summarized the comparison between nominal conditions and predicted results, the nominal operation conditions can be found in [20].

Table 6. Comparison between the predicted values and the operating ones, along with the deviation between the experimental and predicted data as a relative error.

	Trapani plant nominal data	Model predictions	Error (%)
Total distillate mass flow rate [kg/s]	104	101.6	2.5
Motive steam mass flow rate [kg/s]	6.3	6.25	0.8
Compressed flow temperature [°C]	64.5	65.7	1.9
Steam ejector entrainment ratio [-]	1.8	1.7	5.6
Brine mass flow rate (effect 12) [kg/s]	209.7	212.6	1.38
GOR	16.6	16.3	1.8
Vapour temperature [°C]			
Effect 1	62.2	62.0	0.32
Effect 5	53.1	52.9	0.38
Effect 11	39.3	40.6	3.31
Effect 12	37.0	38.2	3.24

As shown in Table 6, the predicted values displayed here are in good agreement (< 6%) with the experimental nominal data. One point worth mentioning is that the recovery of the desalination unit-ratio between the total distillate mass flow rate and the intake seawater mass flow rate - is worth 34%, usually it is less than 40%.
Fig.7 shows the good agreement between the predicted values and nominal experimental data for the pressure in each effect for example.

PRE-PRINT of the paper published on Desalination 452 (2019). Note that it may differ from the final published version (https://doi.org/10.1016/j.desal.2018.10.026) due to several revisions implemented during the peer review process of the journal.

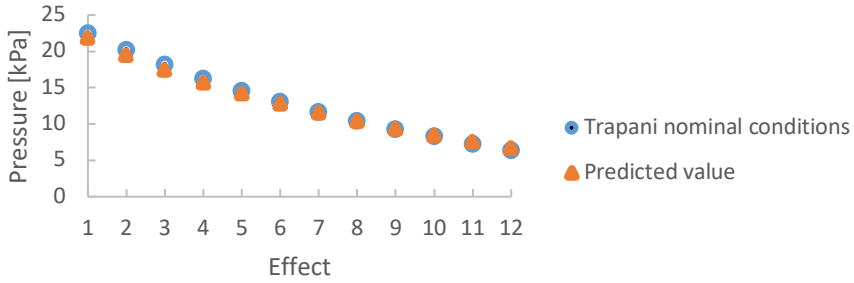

Fig. 7. Comparison between predicted values and experimental ones for the pressure in each effect.

A general overview of the main trends in stationary conditions is given in Fig.8. This stands as the reference case.

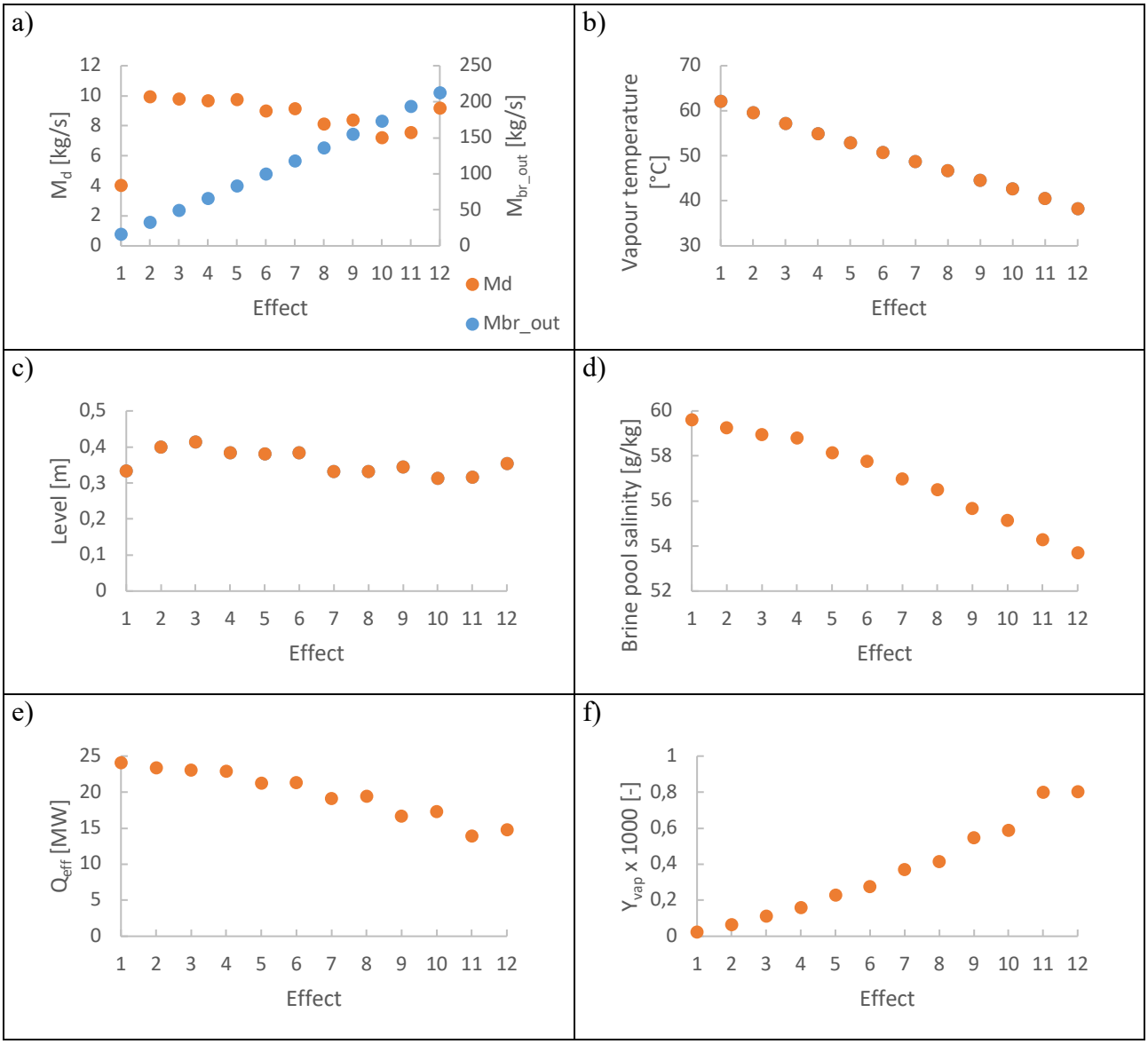

Fig. 8. Overview of the predicted trends of main operating variables. a) distillate and brine mass flow rates; b) vapour temperatures; c) brine pool levels; d) brine pool salinity in each effect; e) heat transfer rate; f) NCG mass fraction in the vapour phases.

PRE-PRINT of the paper published on Desalination 452 (2019). Note that it may differ from the final published version (https://doi.org/10.1016/j.desal.2018.10.026) due to several revisions implemented during the peer review process of the journal.

Those trends are representative of the physical expectations regarding the behaviour of the plant. The distillate mass flow rate (Fig.8.a) tends to decrease with the effect position, which is explained by the fact that the temperature (Fig.8.b) and pressure inside the effects is also decreasing, thus leading to a decrease in the heat transfer rate (Fig.8.e). In addition, the distillate mass flow rate of the first effect is smaller than the other ones as part of the produced vapour is fed to the boilers. The brine mass flow rate (Fig.8.a) increases from the first to the last effect, which is expected as the brine goes from one effect to the next and is only extracted from the last effect, therefore decreasing the brine pool salinity (Fig.8.d) and the brine level in each effect is between 0.3 and 0.5m (Fig.8.c). Finally, the NCG species concentration (Fig.8.f) increases along with the effect position, since they move from one effect to the next, through the pre-heaters until the final condenser where they are extracted.
Once the reference case is set, it is then possible to simulate the plant behaviour under other conditions and to study the dynamic of the plant.

5. Dynamic response of the system and example of a control strategy

Experience in steady-state operating MED plant shows that the hardest variable to control in order to stabilize the plant is the brine levels inside the effects since a slight incoming perturbation can interfere with the brine levels. Besides, changes in the levels can also provoke other perturbations regarding other variables, such as temperature or vapour production rate, and lead to huge instabilities. Finally, as will be shown later, the level has a very slow dynamic and it can take several hours before it is stabilized again. Therefore, it is of major importance to develop a control strategy before considering coupling a MED plant with renewable energies.

When operating a MED-TVC plant, the only operating input are the pressure of the motive steam at the steam ejector and the seawater mass flow rate at the final condenser. Indeed the intake seawater temperature is not controlled and only depends on the season. In order to study the system behaviour under dynamic conditions, several analyses were carried out, firstly by simulating perturbations of the operating variables separately and then altogether.
Firstly, the effects of a step change in the motive steam pressure is studied, as a step decrease of 5.5% is applied to the motive steam pressure. This will lead to almost flooding the effect as will be explained in the first part. Secondly, a step decrease of 3.3% is applied to the intake seawater mass flow rate to study its impact on the plant. Finally, as will be explained in the last part, by combining both those perturbations simultaneously, it is possible to stabilize the plant.

5.1 Effects of a step change in the motive steam pressure (P_p)

Fig.9 displays the effect of a step decrease of 5.5% in the motive steam pressure. The simulation starts from the nominal conditions. This represents a decrease of approximately 4°C in the motive steam temperature that leads to a 1°C decrease in the 1st effect condensation temperature. This value was chosen, so that the 1st effect is almost flooded, as the effect is considered flooded once the brine level reaches 0.6 m. Indeed, the simulation needs to be stopped once the brine level exceeds 0.6 m as it corresponds to when the brine reaches the first row of tubes in the MED plant and it can damage the installation. Furthermore, as shown in section 3.3.2, with the U-pipes model we can perform a simulation with a step increase of 20% in the motive steam pressure without emptying the effects and emptying and flooding are the two main scenarios that can lead to huge instabilities during operation.

PRE-PRINT of the paper published on Desalination 452 (2019). Note that it may differ from the final published version (https://doi.org/10.1016/j.desal.2018.10.026) due to several revisions implemented during the peer review process of the journal.

This is the reason that led us to choose to study what happens when the effect is flooded as it is now more likely to happen.

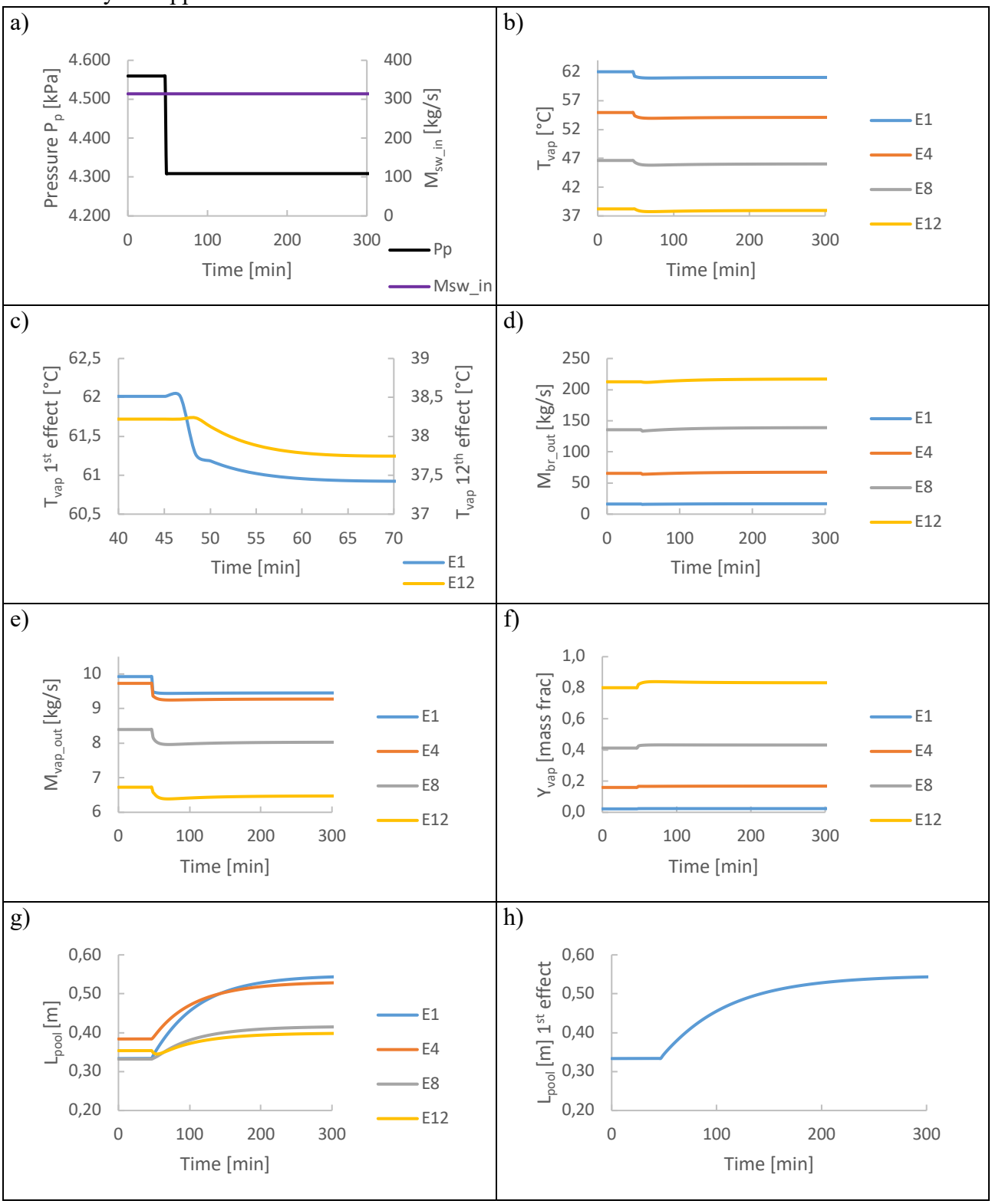

Fig. 9. Transient response of the system to a step change of the motive steam pressure by -5,5% from nominal conditions. a) disturbances in P_p and M_{sw_in}; b) vapour temperature; c) vapour temperature in the first and last effect; d) brine mass flow rate; e) vapour mass flow rate; f) NCG mass fraction in the vapour phase; g) brine pool level; h) brine pool level in the first effect.

PRE-PRINT of the paper published on Desalination 452 (2019). Note that it may differ from the final published version (https://doi.org/10.1016/j.desal.2018.10.026) due to several revisions implemented during the peer review process of the journal.

This perturbation leads to a decrease of the vapour temperature in each effect (Fig 9.b). This is expected, as the incoming vapour temperature is lower, so is the temperature of the vapour produced that is then fed to the condensation zone of the next effect and so on. The dynamic of the temperature is quite fast, as it takes less than 10 minutes for the temperature values to reach a new steady-state. The Fig. 9.c is quite interesting as it shows that the 1st effect is the first to be subjected to the perturbation and the impact is almost instantaneous, but it takes almost 2 minutes to reach the last effect and its impact is less pronounced.
When the motive steam temperature decreases, less vapour can be produced (Fig. 9.e), therefore the level in each effect increases (Fig. 9.g) causing a slight increase in the exiting brine mass flow rate (Fig. 9.d). The impact of the perturbation is stronger in the first effect (Fig.9.b and 9.c), this also explains why the brine pool levels are higher in the first effects. As shown in Fig. 9.h, the dynamic of the brine level is very slow, it takes more than 2 hours to reach a new steady-state. The dynamic of the brine mass flow rate is also slower than the other variables as it strongly depends on the brine levels.
Fig 7.f shows that the mass fraction of NCG in the vapour phase is directly linked to the amount of vapour produced, as the vapour production rate decreases, the NCG mass fraction increases. This is because NCG flow rate is the consequence of the constant make-up flow outgassing toward a lower vapour flow rate.

Table 7 depicts the changes in the performance indicators between the two steady states: the distillate mass flow rate and GOR.

Table 7. Variation of the main performance indicators when the motive steam pressure decreases

	D_{tot} [kg/s]	GOR [-]
Nominal conditions	101.6	16.3
-5,5% P_p	97.1	16.4

As less vapour is produced, less distillate can be obtained, thus reducing the total distillate mass flow rate, resulting however in a higher GOR value as the motive steam mass flow rate has the same variation as the pressure.

5.2 Effects of a step change in the intake seawater mass flow rate (M_{sw_in})

Here is investigated the impact on the MED plant when a reduction of 3.3% is applied to the intake seawater mass flow rate at the inlet of the final condenser. This simulation, like before, starts from nominal conditions. Fig.10 depicts the effect on the different tracked variables.

a)	b)

PRE-PRINT of the paper published on Desalination 452 (2019). Note that it may differ from the final published version (https://doi.org/10.1016/j.desal.2018.10.026) due to several revisions implemented during the peer review process of the journal.

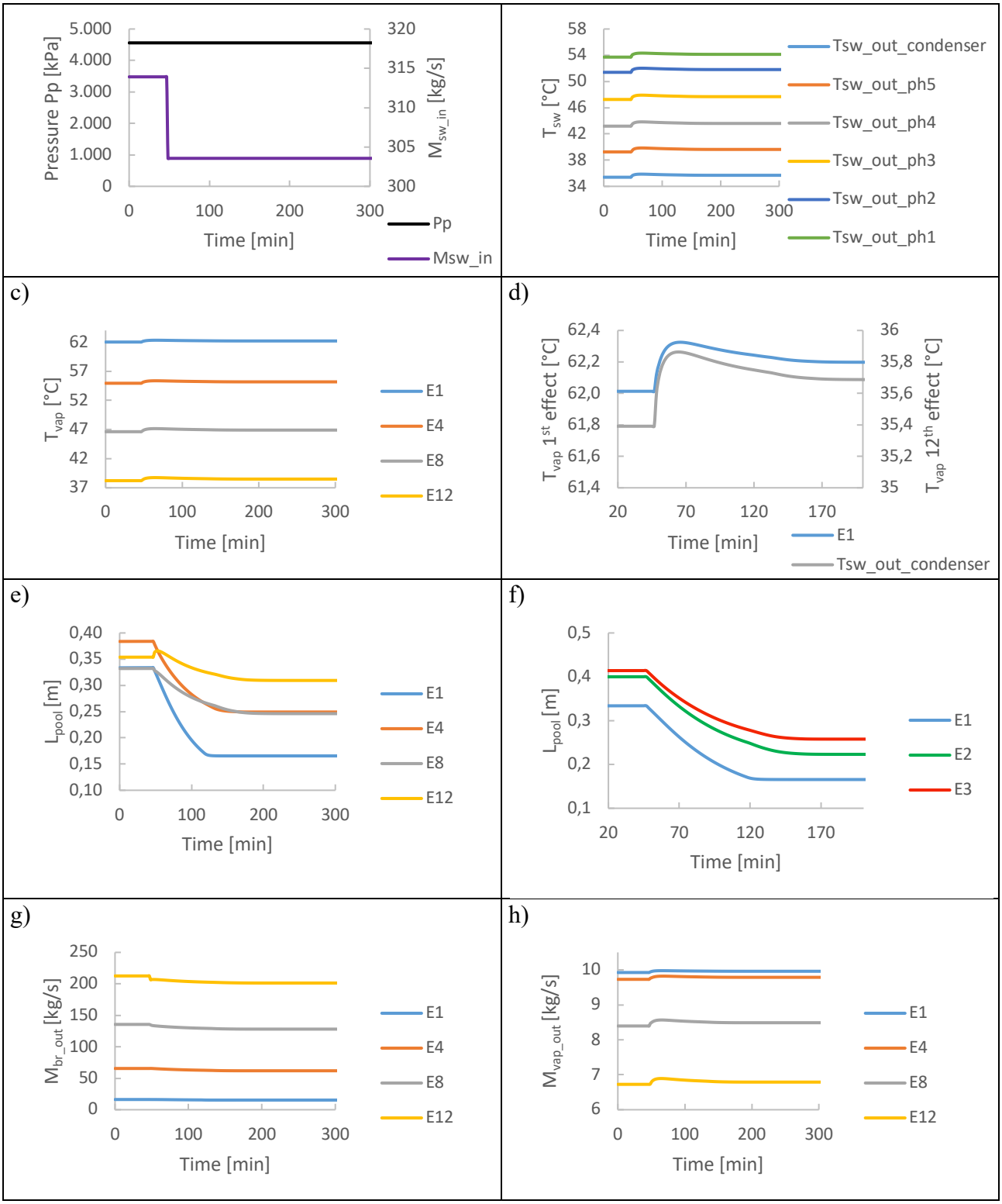

Fig. 10. Transient response of the system to a step change of the seawater mass flow rate by 3.3%, starting in nominal conditions. a) disturbances in P_p and M_{sw_in}; b) feed seawater temperature; c) vapour temperature; d) vapour temperature in the first effect and seawater exiting the final condenser; e) brine pool level; f) brine pool level in the first effect; g) brine mass flow rate; h) vapour mass flow rate.

PRE-PRINT of the paper published on Desalination 452 (2019). Note that it may differ from the final published version (https://doi.org/10.1016/j.desal.2018.10.026) due to several revisions implemented during the peer review process of the journal.

A negative step in the intake seawater mass flow rate leads to an increase in the seawater temperature exiting the final condenser, and consequently the seawater exiting the pre-heaters is slightly warmed up (Fig 10.b). This means that the feeding seawater sprayed across each effect is at a higher temperature and this explains why the temperature inside the effects is also higher (Fig. 10.c). Therefore, it also increases the evaporation rate (Fig. 10.h) as more energy is available for the evaporation process. In this scenario, the vapour temperature in the effect needs more time to reach a new steady state, as it takes also longer to increase the temperature of the intake seawater (Fig. 10.d). As more vapour is produced and less seawater introduced, it leads to a decrease in the brine pool levels (Fig. 10.e) as well as in the brine mass flow rates (Fig. 10.g), as they are both interdependent. The dynamic of the brine levels is faster than in the previous configurations, but it still takes approximately 1 hour to reach a new steady state (Fig. 10.f). Another interesting conclusion is regarding the slope of the brine level in the first effect (Fig. 10.f). Indeed, it changes abruptly and stabilizes almost instantly after decreasing during 1 hour. The moment where the level stabilizes corresponds to the exact moment when the brine pool level in the second effect becomes inferior to the weir height, this result shows the importance of the weir height in the stabilization process. In addition, the level in the third effect is superior to the weir height, which is why the level in the third effect has a curvier aspect.

Small variations between the two steady states are also reflected in the new values of the performance indicators in Table 8.

Table 8. Variation of the main performance indicators when the inlet seawater mass flow rate decreases

	D_{tot} [kg/s]	GOR [-]
Nominal conditions	101.6	16.3
-3.3% M_{sw_in}	102.6	16.4

As the evaporation process is slightly more efficient, the total distillate mass flow rate is a little higher and the GOR slightly increases. This result can be explained by the fact the pressure is higher in the effects, so is the entrained steam pressure and mass flow rate at the ejector, as it comes from the last effect, but the motive steam pressure at the steam ejector is maintained constant, thus so is the motive steam mass flow rate. Therefore, the compressed steam mass flow rate is higher and more vapour is condensed in the first effect, releasing more latent heat, consequently leading to a higher vapour production rate in the first effect and this is repeated in the following effects. In consequence, the total distillate mass flow rate increases and so does the GOR.

5.3 Establishing a control strategy by acting simultaneously on P_p and M_{sw_in}

5.3.1 Effects of a step change in the motive steam pressure and the intake seawater mass flow rate

The response of the MED plant to step changes in the two operating variables has been previously detailed separately. This highlighted that they both have counteracting effects, thus leading to conclude that it could be possible to stabilize the MED-TVC plant by acting simultaneously on those two variables. Therefore, here is studied what happens when those two perturbations occur at the same time, starting from nominal conditions. Fig. 11 depicts the effects of decreasing the motive

PRE-PRINT of the paper published on Desalination 452 (2019). Note that it may differ from the final published version (https://doi.org/10.1016/j.desal.2018.10.026) due to several revisions implemented during the peer review process of the journal.

steam pressure by 5.5% and the intake seawater mass flow rate by 3.3% at the same time on the other variables.

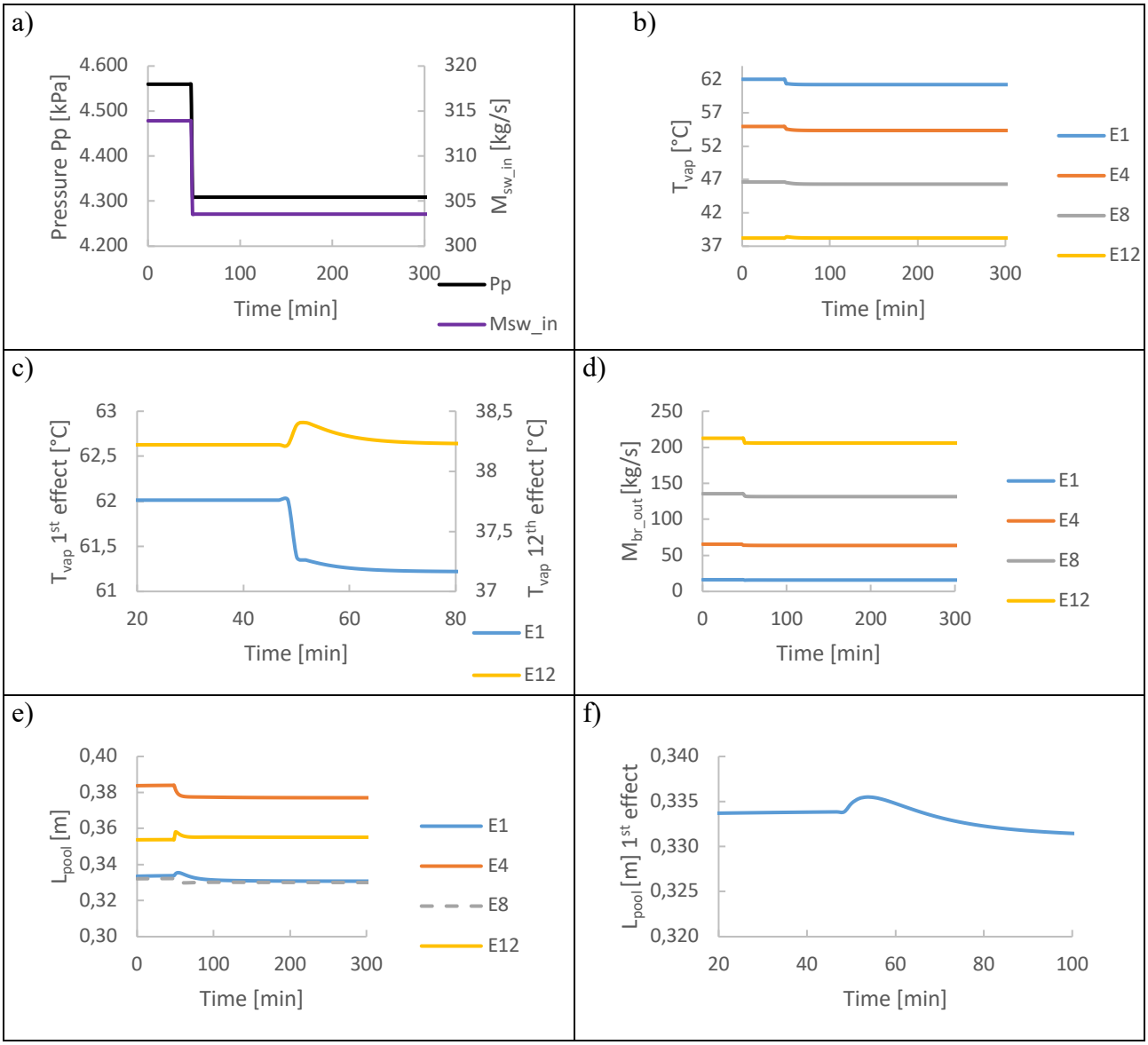

Fig. 11. Transient response of the system to a simultaneous variation of the motive steam pressure and inlet seawater mass flow rate, starting in nominal conditions; a) disturbances in P_p and M_{sw_in}; b) vapour temperature; c) vapour temperature in the first and last effect; d) brine mass flow rate; e) vapour mass flow rate; f) NCG mass fraction in the vapour phase; g) brine pool level; h) brine pool level in the first effect.

When applying both perturbations simultaneously, each variable reaches rapidly a new steady state. The temperatures in the effects tend to slightly decrease (Fig. 11.b), except for the vapour temperature in the last effect that is increased (Fig. 11.c). This is explained by the fact that, as seen in section 5.1, it takes about 2 minutes for the perturbation of the motive steam pressure to reach the last effect, whereas, as it is close to the final condenser, it is immediately subjected to the seawater mass flow rate variation. Thus, the temperature increases at first, but then after 2 minutes it decreases and stabilizes around the same value as before. The impact of the motive steam pressure is stronger on the temperature than the intake seawater mass flow rate variation, as the variation of pressure is more

important than the one of seawater mass flow rate, therefore, the vapour temperatures are diminishing, but their variations are smaller than those obtained when only the motive steam pressure changes. At first sight, the brine levels are subjected to small variations when the perturbations occur but go back close to their initial states when the new steady-state is reached (Fig. 11.e). When looking more closely (Fig. 11.f), one can observe that the brine level increases because of the variation in the motive steam pressure but after less than 10 minutes, the seawater mass flow rate variation counterbalances the effect of the pressure and the brine level decreases again. The brine levels reach a new steady-state after less than 20 minutes, so it is much faster than the 2 hours required in the first scenario. The brine mass flow rates (Fig.11.d) are subjected to small changes, directly linked to the brine levels' variations.

In consequence, the variations in the performance indicators between the two steady states are shown in Table 9.

Table 9. Variation of the main performance indicators to a simultaneous decrease in the inlet seawater mass flow rate and motive steam pressure

	D_{tot} [kg/s]	GOR [-]
Nominal conditions	101.6	16.3
-5.5% P_p & -3.3% $M_{sw\ in}$	98.0	16.6

The motive steam pressure variation has a greater impact on the total distillate mass flow rate than the seawater mass flow rate change, which is the reason why the value is smaller at the end of the simulation, but it still is higher than in the 1st case scenario. Thus, the GOR value is also changed and increases.

5.3.2 Another example of possible simulations with those new considerations

Before implementing the new points described in this paper, there were some major limitations regarding the possible disturbances that could be studied. Here is presented an extreme example, which is what happens when the motive steam pressure is suddenly decreased by 40% and the intake seawater mass flow rate by 27% to show the importance and robustness of the control strategy. This simulation shows the enormous range of possible simulations that we can now study with this new model. For this reason and because the brine levels are the most critical, due to their very slow dynamic, and they are the most important variables regarding the dynamic study of the MED plant, Fig.12. shows only the brine levels evolutions in the effects.

a)	b)

PRE-PRINT of the paper published on Desalination 452 (2019). Note that it may differ from the final published version (https://doi.org/10.1016/j.desal.2018.10.026) due to several revisions implemented during the peer review process of the journal.

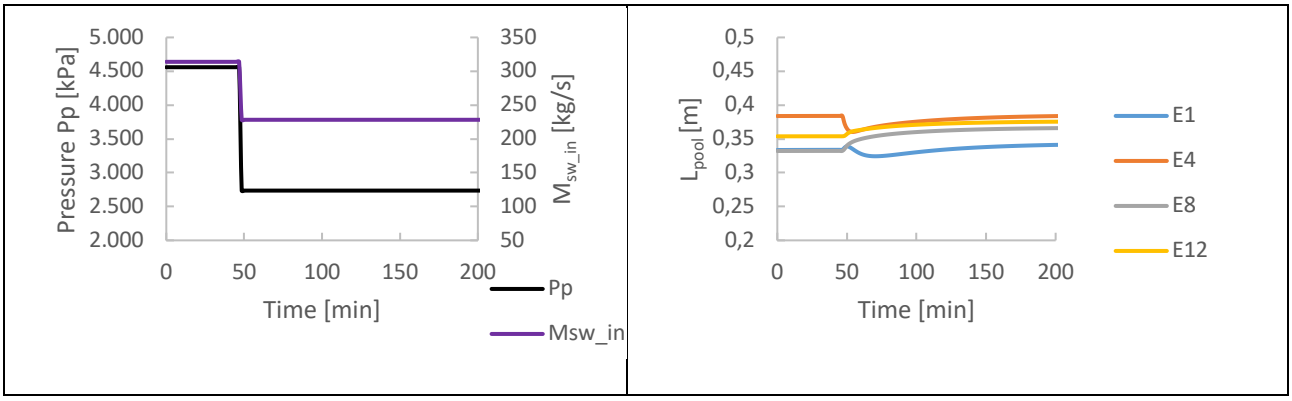

Fig. 12. Transient response of the system for the following disturbances: -40% P_p and -27% M_{sw_in}

Much larger disturbances are shown in Fig.12 and even under those extreme conditions, the simulation is able to run and is reliable to describe what happens in the MED plant. The brine pool levels reach a new steady-state in less than 30 minutes which is close to the initial state (Fig. 12.b). Which confirms the fact that with the improvements presented in this paper as well as with the development of a control strategy, it is now possible to study the dynamic behaviour of the plant against very wide variations of the main operational inputs.

6. Conclusion

This article presents new considerations for modelling a MED-TVC plant under dynamic conditions. The model presented in this paper was implemented using two different software, gPROMS® and MATLAB®, and validated with real operating data in steady-state from a MED-TVC plant located in Trapani, Sicily (Italy). This work highlights the importance to take into consideration every phenomenon that occur, with as few assumptions as possible, but also to correctly describe the interconnection between the effects as they play a significant role in the plant behaviour, especially under dynamic conditions. With those new implementations, the mathematical description of the model is more accurate and faithful to the real operation of a MED-TVC plant. Indeed, as in a real plant, the only inputs variables are the motive steam pressure and the intake seawater mass flow rate at the final condenser, thus addressing several modelling gaps present in the literature.
This model was used to perform dynamic simulations to study the behaviour of the plant under those conditions. It proved the high sensibility of the brine level variations leading to the flooding/emptying of the effect. Therefore, an example of a control strategy is described in order to maintain a high-level stability, even under transient conditions, thus proving the feasibility of coupling a MED plant with a fluctuating heat source.

Acknowledgments

The authors wish to thank the European Commission (DG for Research & Innovation) for its financial assistance within the Integrated Research Programme in the field of Concentrated Solar Power (CSP) (STAGE-STE Project; Grant Agreement No. 609837). Siciliacque SpA and the plant manager, Mr. Carmelo Mineo, are warmly thanked for providing the operating data of the Trapani plant and for the highly valuable advices helping significantly the understanding of the real plant operations and design. Finally, the authors would like to thank the InnoEnergy PhD School program which funded the mobility that led to this successful and fruitful collaboration between the French Alternative

PRE-PRINT of the paper published on Desalination 452 (2019). Note that it may differ from the final published version (https://doi.org/10.1016/j.desal.2018.10.026) due to several revisions implemented during the peer review process of the journal.

Energies and Atomic Energy Commission (CEA), the University of Lyon Claude Bernard 1 and the University of Palermo.

Nomenclature

A	surface [m^2]
A_{mat}	Matrix A
Ar	Archimedes number [-]
B	mass of brine [kg]
BPE	boiling point elevation [°C]
Cd	brine discharge coefficient [-]
C_G	gas solubility [µmol/kg]
Cp	specific heat [J/(kg·°C)]
D	diameter [m]
D_{tot}	total distillate production [kg/s]
g	specific gravity [m/s^2]
GOR	Gain Output Ratio [-]
G_{pool}	gain in brine flow-rate control equation[kg/(m·s)]
H	enthalpy [J]
h	specific enthalpy [J/kg]
H_c	Henry-like constant [Pa]
H_{pipe}	height of the U-pipe for circulation of the brine between two effects [m]
h_w	weir height of the U-pipe [m]
k	thermal conductivity [W/(m.K)]
L	length of the effect [m]
LMTD	logarithmic mean temperature difference [°C]
L_{pool}	brine level [m]
M	mass flow rate [kg/s]
NCG	mass of non-condensable gas [kg]
Nu	Nusselt number [-]
P	pressure [Pa]
PM	molar weight [kg/mol]
Pr	Prandtl number [-]
Q	heat flux [W]
R	ideal gas constant [J/mol K]
Re	Reynolds number [-]
S	auxiliary salinity [kg.ppm]
T	temperature [°C]
U	heat transfer coefficient [$W/(m^2 .K)$]
Vap	mass of the vapour phase [kg]
Vol	volume [m^3]
X	mass fraction of non-condensable species in the liquid phase
X_{mat}	State vector
x	salt concentration expressed as [ppm]
Y	mass fraction of non-condensable species in the vapour phase

Greek letters

PRE-PRINT of the paper published on Desalination 452 (2019). Note that it may differ from the final published version (https://doi.org/10.1016/j.desal.2018.10.026) due to several revisions implemented during the peer review process of the journal.

α	equivalent vapour discharge coefficient [m^2]
Γ	liquid mass flow rate per unit length of tube [kg/(m.s)]
Δ	difference
ε	condensation ratio in the tube bundle [-]
θ	release coefficient of non-condensable gas [-]
λ	latent heat [J/kg]
μ	dynamic viscosity [kg/(m.s)]
ρ	density [kg/m^3]
ν	kinematic viscosity [m^2/s]

Subscript

air	air
br_in	brine stream arriving from the previous effect
br_out	brine stream leaving the effect to the following one
br_shell	dispersed liquid reaching the brine pool from the tube bundle
cond	condensation
d	condensed vapour exiting the tube bundle
ds	De-super-heater
eff	effective quantity of heat transferred
eq	equilibrium
evap	evaporation
ext	external
f	feed seawater sprayed over the tube bundle
flash	vapour generated by the flashing of brine arriving from previous effect
in	inlet
int	internal
mix	vapour and non-condensable gases mixture
mol	molar fraction
ms	motive steam (i.e. condensing vapour) entering the tube bundle
NCG	non-condensable gas
NCG_entrained	NCG arriving to the effect from the previous effect
NCG_entrained_ph	NCG entrained from one effect to the pre-heater
NCG_pool	NCG released from the brine arriving from the previous effect
NCG_shell	NCG released from the dispersed brine around the tube bundle
out	outlet
p	motive steam to the ejector
ph	pre-heater
phase	phase in the effect (number 1, 2 or 3)
pipe	tube connection between two effects

PRE-PRINT of the paper published on Desalination 452 (2019). Note that it may differ from the final published version (https://doi.org/10.1016/j.desal.2018.10.026) due to several revisions implemented during the peer review process of the journal.

pool	brine accumulated in the pool
ref	reference state for calculation
SE	single evaporation effect
shell	brine around tube bundle
sp	set point fixed for the brine pool level
sw	seawater
sw_in	seawater entering the condenser
sw_in_ph	seawater entering the pre-heater
sw_out	seawater exiting from the condenser
sw_out_ph	seawater exiting from the pre-heater
tubes	tubes
vap	vapour phase
vap_out	gas mixture exiting the effect
w	tube wall

List of Abbreviations

BPE	boiling point elevation
MED	multiple-effect distillation
MSF	Multi stage Flash
NCG	non-condensable gas
NEA	non-equilibrium allowance
SE	single effect
TVC	thermal vapour compression

APPENDIX I

Auxiliary equations for heat transfer calculations and thermodynamic properties

Water enthalpy of vaporization [27]

$$\lambda = \left(2501.897149 - 2.407064037 \cdot T + 1.192217 \cdot 10^{-3} \cdot T^2 - 1.5863 \cdot 10^{-5} \cdot T^3\right) \cdot 10^3 \quad \text{I.1}$$

Boiling Point Elevation [5]

$$BPE = BPE_1 \cdot \left(x \cdot 10^{-4}\right) + BPE_2 \cdot \left(x \cdot 10^{-4}\right)^2 + BPE_3 \left(x \cdot 10^{-4}\right)^3 \quad \text{I.2}$$

$$BPE_1 = \left[8.325 \cdot 10^{-2} + 1.883 \cdot 10^{-4} \cdot T + 4.02 \cdot 10^{-6} \cdot (T)^2\right] \quad \text{I.3}$$

$$BPE_2 = \left[- 7.625 \cdot 10^{-4} + 9.02 \cdot 10^{-5} \cdot T - 5.2 \cdot 10^{-7} \cdot (T)^2\right] \quad \text{I.4}$$

$$BPE_3 = \left[1.522 \cdot 10^{-4} - 3 \cdot 10^{-6} \cdot T - 3 \cdot 10^{-8} \cdot (T)^2\right] \quad \text{I.5}$$

PRE-PRINT of the paper published on Desalination 452 (2019). Note that it may differ from the final published version (https://doi.org/10.1016/j.desal.2018.10.026) due to several revisions implemented during the peer review process of the journal.

Non-equilibrium allowance [5]

$$NEA=33 \cdot \frac{(\Delta T_{pool,i})^{0.55}}{T_{vap,i}} \quad \text{I.6}$$

Overall heat transfer coefficient for the final condenser and preheaters [5]

$$U = 1.7194+3.2063\cdot10^{-3}\cdot T_{vap}+1.5971\cdot10^{-5}\cdot T_{vap}^{2}+ 1.9918\cdot10^{-7}\cdot T_{vap}^{3} \quad \text{I.7}$$

The above equation was developed over a temperature range of 40 to 120°C.

Heat transfer coefficient for the condensation inside the tube bundle developed by Chato [24]

$$U_{cond} = 0.555 \cdot \left(\frac{\rho_{cond} \cdot (\rho_{cond} - \rho_{vap}) \cdot g \cdot k_{cond}^{3} \cdot \lambda_{cond}}{D_{tubes\_int} \cdot \mu_{cond} \cdot (T_{cond} - T_{w})} \right)^{1/4} \quad \text{I.8}$$

The above correlation is recommended for Re < 35000.

APPENDIX II

Mathematical model of the steam ejector

This model was already presented by El-Dessouky *et al.* in 2002 [9], and has been modified according to a reference textbook on Fluid Mechanics [28].
All the equations presented here refer to the simplified scheme of a typical steam ejector adopted in MED-TVC units, as reported in Figure II. 1.

PRE-PRINT of the paper published on Desalination 452 (2019). Note that it may differ from the final published version (https://doi.org/10.1016/j.desal.2018.10.026) due to several revisions implemented during the peer review process of the journal.

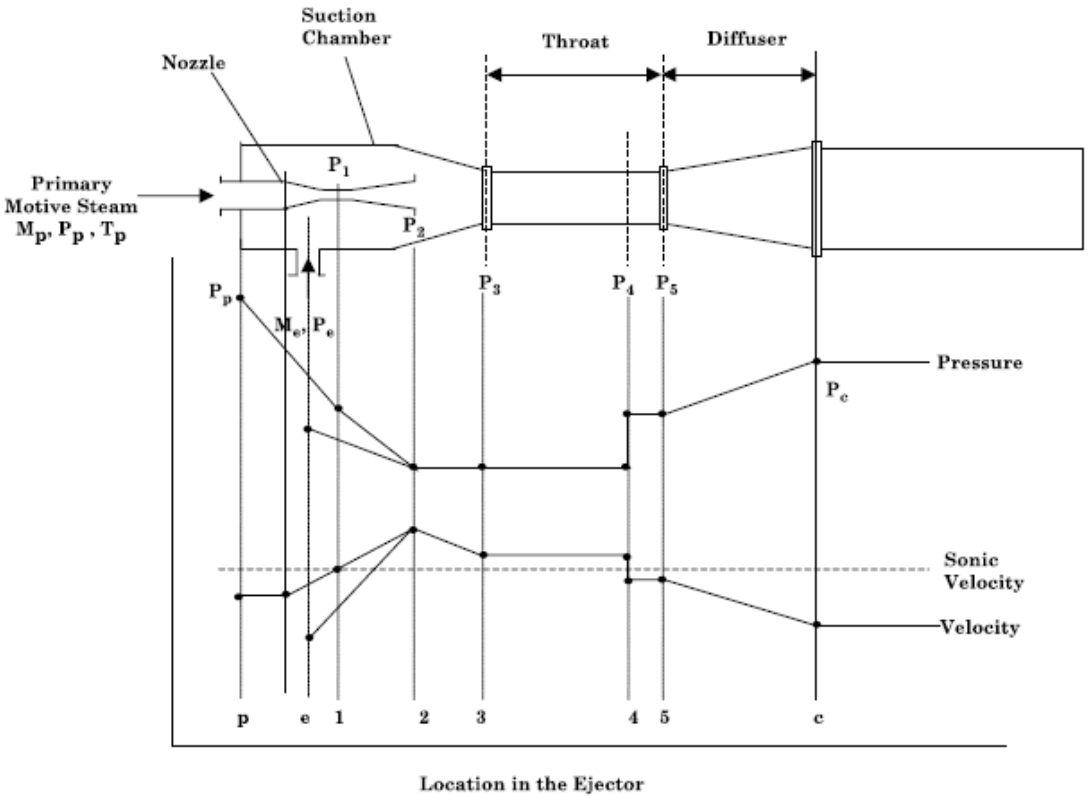

Fig. II.1. Simplified scheme of a steam ejector. Source : [9]

Overall material balance:

$$mp + me = mc \qquad \text{II.1}$$

M stands for the mass flow rate and the subscripts p, e, c are respectively for motive, entrained and compressed steam.

Entrainment ratio:

$$w = \frac{me}{mp} \qquad \text{II.2}$$

Mach number of the primary fluid at the nozzle outlet (after the isentropic expansion):

$$M_{p2} = \sqrt{\frac{2\eta_n}{\gamma-1}\left[\left(\frac{P_p}{P_2}\right)^{\frac{\gamma-1}{\gamma}} - 1\right]} \qquad \text{II.3}$$

Where η_n is the nozzle efficiency, γ is the compressibility ratio, P is the pressure.

Mach number of entrained fluid flow at the nozzle exit (after the isentropic expansion):

$$M_{e2} = \sqrt{\frac{2}{\gamma-1}\left[\left(\left(\frac{P_e}{P_2}\right)^{\frac{\gamma-1}{\gamma}}\right) - 1\right]} \qquad \text{II.4}$$

Critical Mach number after the mixing of entrained and motive steams:

PRE-PRINT of the paper published on Desalination 452 (2019). Note that it may differ from the final published version (https://doi.org/10.1016/j.desal.2018.10.026) due to several revisions implemented during the peer review process of the journal.

$$M_4^* = \frac{M_{p2}^* + \left[\omega \cdot M_{e2}^* \cdot \left(\frac{T_e}{T_p}\right)^{0.5}\right]}{\sqrt{(1+\omega)\cdot\left(1+\frac{\omega T_e}{T_p}\right)}} \qquad \text{II.5}$$

T is for the temperature and M* stands for the critical Mach number. The latter is related to the Mach number with equation II.6

$$M^* = \sqrt{\frac{M^2\cdot(\gamma+1)}{[M^2\cdot(\gamma-1)]+2}} \qquad \text{II.6}$$

Mach number of the mixed stream after the shock wave (position 5 of the scheme in Fig.II. 1):

$$M_5^2 = \frac{M_4^2 + \frac{2}{\gamma-1}}{\frac{2\gamma}{\gamma-1}\cdot M_4^2 - 1} \qquad \text{II.7}$$

Pressure increase after the shock wave (positions 4-5 of the scheme in Fig.II. 1):

$$P_5 = P_4 \frac{1+\gamma\cdot M_4^2}{1+\gamma\cdot M_5^2} \qquad \text{II.8}$$

The pressure is assumed constant along the ejector tube so P_4 is equal to P_2.

Pressure rise in the diffuser (positions 5-c of the scheme in Fig.II. 1):

$$P_c = P_5\cdot\left[\frac{\eta_d\cdot(\gamma-1)\cdot M_5^2}{2}+1\right]^{\frac{\gamma}{\gamma-1}} \qquad \text{II.9}$$

The section of the nozzle throat:

$$A_1 = \frac{m_p}{P_p}\cdot\sqrt{\frac{R\cdot T_p}{\gamma\cdot\eta_n}\left(\frac{\gamma+1}{2}\right)^{\frac{\gamma+1}{\gamma-1}}} \qquad \text{II.10}$$

The section ratio between the nozzle throat and the nozzle outlet:

$$\frac{A_2}{A_1} = \sqrt{\frac{1}{M_{p2}^2}\cdot\left(\frac{2}{\gamma+1}\cdot\left(1+\frac{(\gamma-1)}{2}M_{p2}^2\right)\right)^{\frac{\gamma+1}{\gamma-1}}} \qquad \text{II.11}$$

Finally, the ratio between the nozzle and the diffuser:

PRE-PRINT of the paper published on Desalination 452 (2019). Note that it may differ from the final published version (https://doi.org/10.1016/j.desal.2018.10.026) due to several revisions implemented during the peer review process of the journal.

$$\frac{A_1}{A_3} = \frac{P_c}{P_p} \cdot \sqrt{\frac{1}{(1+\omega)\left(1+\left(\omega\left(\frac{T_e}{T_p}\right)\right)\right)}} \cdot \frac{\left(\frac{P_2}{P_c}\right)^{\frac{1}{\gamma}} \cdot \sqrt{1-\left(\frac{P_2}{P_c}\right)^{\frac{\gamma-1}{\gamma}}}}{\left(\frac{2}{\gamma+1}\right)^{\frac{1}{\gamma-1}} \cdot \sqrt{1-\left(\frac{2}{\gamma+1}\right)}} \qquad \text{II.12}$$

where A_1, A_2 and A_3 are the cross sections of the nozzle throat, the nozzle exit and the diffuser constant section, respectively.

As said before, those equations were first used to define A1, A2 and A3 with operation data as inputs (as reported in Table II.1).

Table II.1 Set of experimental values and determined geometrical parameters of the TVC ejector

Set values		Design parameters	
ω	0.58	A_1	0.00109 m^2
P_p	$4.5 \cdot 10^6$ Pa	A_2	0.05607 m^2
P_e	$6 \cdot 10^3$ Pa	A_3	0.60707 m^2
P_c	$2.53 \cdot 10^4$ Pa		
γ	1.33		
η_d	0.85		
η_n	0.85		
R	461 J/(kg·K)		
m_c	9.86 kg/s		

Nomenclature for Appendix II

A	cross section area [m^2]
M	Mach number
M^*	critical Mach number
m	mass flow rate [kg/s]
P	pressure [Pa]
R	universal gas constant [J/kg K]
T	temperature [K]

Greek symbols

γ	compressibility ratio
η	ejector efficiency
ω	entrainment ratio

PRE-PRINT of the paper published on Desalination 452 (2019). Note that it may differ from the final published version (https://doi.org/10.1016/j.desal.2018.10.026) due to several revisions implemented during the peer review process of the journal.

Subscript

1-5	positioning of sections within the ejector scheme
c	compressed vapour
d	diffuser
e	entrainment vapour
n	nozzle
p	motive steam

References

[1] Unesco, ed., Facing the challenges, UNESCO, Paris, 2014.
[2] Unesco, ed., Water for a sustainable world, UNESCO, Paris, 2015.
[3] P. Bandelier, Le dessalement d'eau de mer et des eaux saumâtres, (2016).
[4] A. Cipollina, M. Agnello, A. Piacentino, A. Tamburini, B. Ortega, P. Palenzuela, D. Alarcon, G. Micale, A dynamic model for MED-TVC transient operation, Desalination. 413 (2017) 234–257. doi:10.1016/j.desal.2017.03.005.
[5] H.T. El-Dessouky, H.M. Ettouney, Fundamentals of salt water desalination, Elsevier, 2002.
[6] H.T. El-Dessouky, H.M. Ettouney, Multiple-effect evaporation desalination systems. Thermal analysis, Desalination. 125 (1999) 259–276.
[7] H.T. El-Dessouky, H.M. Ettouney, F. Al-Juwayhel, Multiple effect evaporation—vapour compression desalination processes, Chem. Eng. Res. Des. 78 (2000) 662–676.
[8] H. El-Dessouky, I. Alatiqi, S. Bingulac, H. Ettouney, Steady-state analysis of the multiple effect evaporation desalination process, Chem. Eng. Technol. 21 (1998) 437.
[9] H. El-Dessouky, H. Ettouney, I. Alatiqi, G. Al-Nuwaibit, Evaluation of steam jet ejectors, Chem. Eng. Process. Process Intensif. 41 (2002) 551–561.
[10] A.M. El-Nashar, A. Qamhiyeh, Simulation of the performance of MES evaporators under unsteady state operating conditions, Desalination. 79 (1990) 65–83.
[11] N.H. Aly, M.A. Marwan, Dynamic response of multi-effect evaporators, Desalination. 114 (1997) 189–196.
[12] S. Dardour, S. Nisan, F. Charbit, Development of a computer-package for MED plant dynamics, Desalination. 182 (2005) 229–237. doi:10.1016/j.desal.2005.02.028.
[13] L. Roca, L.J. Yebra, M. Berenguel, D.C. Alarcón-Padilla, Modeling of a Solar Seawater Desalination Plant for Automatic Operation Purposes, J. Sol. Energy Eng. 130 (2008) 041009. doi:10.1115/1.2969807.
[14] M.T. Mazini, A. Yazdizadeh, M.H. Ramezani, Dynamic modeling of multi-effect desalination with thermal vapor compressor plant, Desalination. 353 (2014) 98–108. doi:10.1016/j.desal.2014.09.014.
[15] A. de la Calle, J. Bonilla, L. Roca, P. Palenzuela, Dynamic modeling and performance of the first cell of a multi-effect distillation plant, Appl. Therm. Eng. 70 (2014) 410–420. doi:10.1016/j.applthermaleng.2014.05.035.

[16] A. de la Calle, J. Bonilla, L. Roca, P. Palenzuela, Dynamic modeling and simulation of a solar-assisted multi-effect distillation plant, Desalination. 357 (2015) 65–76. doi:10.1016/j.desal.2014.11.008.
[17] L. Roca, J. Sánchez, F. Rodríguez, J. Bonilla, A. de la Calle, M. Berenguel, Predictive Control Applied to a Solar Desalination Plant Connected to a Greenhouse with Daily Variation of Irrigation Water Demand, Energies. 9 (2016) 194. doi:10.3390/en9030194.
[18] S. Azimibavil, A. Jafarian Dehkordi, Dynamic simulation of a Multi-Effect Distillation (MED) process, Desalination. 392 (2016) 91–101. doi:10.1016/j.desal.2016.04.004.
[19] A. Cipollina, G. Micale, L. Rizzuti, A critical assessment of desalination operations in Sicily, Desalination. 182 (2005) 1–12. doi:10.1016/j.desal.2005.03.004.
[20] C. Temstet, G. Canton, J. Laborie, A. Durante, A large high-performance MED plant in Sicily, Desalination. 105 (1996) 109–114.
[21] H. Glade, K. Genthner, The problem of Non-condensable gas release in evaporators, Desalination. 49 (2000) 357–365.
[22] S. I. Sandler, Chemical and Engineering Thermodynamics, third edition, Wiley and Sons, (1999).
[23] B. Glazer, Didactical Material on "Dissolved Gases Other Than Carbon Dioxide in Seawater", Course of "Chemical Oceanography", School of Ocean and Earth Science and Technology of the University of Hawai'i at Manoadownloaded on the 6th of July 2015 from the link:http://www.soest.hawaii.edu/oceanography/glazer/PDFs/Courses/OCN623/Lectures/Non_CO2_gases-2014-Handouts.pdf.
[24] J.C. Chato, Laminar condensation inside horizontal and inclined tubes, ASHRAE J 4. (1962) 52–60.
[25] G. Ribatski, A.M. Jacobi, Falling-film evaporation on horizontal tubes—a critical review, Int. J. Refrig. 28 (2005) 635–653. doi:10.1016/j.ijrefrig.2004.12.002.
[26] V. Sernas, Heat transfer correlation for subcooled water films on horizontal tubes, J Heat Transf. 101. (1979) 176–178.
[27] R.H. Perry, Perry's chemical engineers' handbook, 6th edition, (2005).
[28] Frank M. White, Fluid Mechanics, 4th Edition, Mc-Graw-Hill (1998) ISBN: 978-0072281927.